




# a

ELOI PALLARÈS ABRIL

m w

# Abstract

This master's thesis conducts investigations on the activation and radiation exposure of crucial components of the SUNRISE-LFR. The primary focus centres on neutron activation in the reactor's internal structures, reactor vessel and steam generators, with particular attention to novel materials such as FeCrAl and AFA stainless steel. Through rigorous simulations and analysis, we have identified niobium-94 as the dominant isotope responsible for the specific external gamma and x-ray dose rate in materials composed of Fe-10Cr-4Al-RE (FeCrAl) [1], such as the internal structures and the main body of the steam generator. In the case of the reactor vessel, iron-55 has been found to determine the cooling time, while manganese-54 dominates in materials comprising Alumina-Forming-Austenitic (AFA) [2]. It is noteworthy that, despite most materials showing a specific activity greater than the clearance limit stipulated in [3], their specific external gamma and x-ray dose rates are extremely low. Moreover, we explore the neutron and high-energy photon flux outside the reactor, revealing higher levels along the lateral reactor portion compared to the top. Specifically, the observed neutron flux reaches approximately $10^8$ neutrons$\cdot$cm$^{-2}\cdot$s$^{-1}$ for the lateral part of the reactor and $10^6$ neutrons $\cdot$ cm$^{-2}$ $\cdot$ s$^{-1}$ on top of the reactor. Meanwhile, no high-energy photons have been detected outside the reactor. Overall, this master's thesis provides valuable insights into reactor safety, structural component handling, and strategies for implementing radiation protection in the SUNRISE-LFR. The outcomes serve as a foundation for future research endeavours, guiding advancements in nuclear reactor design and promoting sustainable electricity generation with enhanced safety standards.

# Acknowledgements

I want to thank everyone in my life right now, thank you from the bottom of my heart for helping me become the person I am right now.

I would like to start my acknowledgements by thanking my supervisor, Fredrik Dehlin. His exceptional guidance, valuable advice, and unwavering support throughout the entire thesis have been truly vital in its success. Fredrik's brilliance and friendship have made this academic endeavour both enriching and fulfilling.

I am deeply thankful to Professor Janne Wallenius for providing me with the unique opportunity to take part in the innovative and revolutionary SUNRISE project and for letting me use his office.

To my beloved family, my parents Jordi and Eva, and my siblings Guim and Rita, for not giving up on me after so many years of crisis due to my studies. Moltes gràcies.

I would also like to extend my appreciation to all my friends from Sweden and France, who have made these years unforgettable and life-changing. Moreover, to all my friends and best friends in Igualada and other parts of Catalonia and Spain who, despite not seeing them for months, always welcome me with their arms open and a big smile on their faces.

While the list of those deserving gratitude could go on indefinitely, I understand the reader's interest in nuclear reactors and not my personal life. Therefore, I hope you enjoy my biggest project to date.

# Contents

# List of Figures

# Chapter 1

# Introduction

It is a well-known fact that climate change is a reality. A meta-study from 2016 [4] showed high scientific consensus on *anthropogenic global warming* (AGW), with agreement ranging between 90% to 100% on AGW. Regarding public opinion: the biggest global poll on climate, with 1.22 million people of all genders, ages, nationalities and educational backgrounds took place in 2021 [5] and it showed that 64% of respondees consider climate change as a global emergency.

The imperative to address the climate crisis has become an undeniable reality. Human civilization, among many things, must transition towards a more sustainable energy mix in order to mitigate the negative consequences associated with the utilization of fossil fuels. While renewable energy sources hold promise, their intermittent nature poses a significant challenge. Hydroelectric power, the exception to this intermittency issue, presents its own drawback in the form of substantial environmental impact on local ecosystems [6]. A study published in 2022 [7] presents a potential pathway towards achieving a 100% renewable energy system by 2050. However, the authors identify three key challenges associated with the full realization of a renewable energy scenario: the protracted timeline required for infrastructure development (spanning approximately three decades), the relatively low energy density of renewable sources, and the intricate relation between intermittency and storage.

An appropriate solution to the aforementioned problem is the combined use of renewables and nuclear fission energy[1]. The combined use of the stated technologies

[1]Nuclear fission obtains energy from splitting a heavy atomic nucleus such as uranium-235.

can solve most of the problems we are facing today. A study performed by the International Energy Agency (IEA) in 2019 [8] concluded that the combined use of renewables and nuclear energy is the best solution to mitigate climate change. This study showed that over 60 gigatonnes of carbon dioxide ($CO_2$) emissions have **not** been emitted thanks to the use of nuclear power during the last 50 years. Even though this quantity seems enormous, it only accounts for two years' worth of global energy-related emissions. Given these results, the IEA concluded in [8] the importance of nuclear power and supports the construction of new nuclear reactors while simultaneously trying to extend the lifetime of existing reactors. Additionally, IEA also encourages investment in small modular reactor (SMR) technologies and Generation IV (GenIV) reactors[2].

Nuclear energy is a well-known and proven technology, with its origin tracing back to the construction of the pioneering experimental nuclear reactor known as the *Chicago Pile-I* by Enrico Fermi and his team in 1942 [9]. December 2nd of that same year, the Chicago Pile-I accomplished a significant milestone as the nuclear reaction became self-sustaining, marking the beginning of the nuclear age. The next major achievement in the history of nuclear energy occurred in June of 1954, 110 km southwest of Moscow, Russia (then Soviet Union), as the first commercial nuclear power plant in the world was connected to the grid in Obninsk, *Science City*. The APS-1 Obninsk (Atomic Power Station 1 Obninsk) Nuclear Power Plant operated for 5 years and ceased its commercial energy production in 1959 but continued to operate as an experimental nuclear reactor until 2002 [10]. Presently, 69 years into the nuclear age, humanity has accumulated over 18 000 years of cumulative experience in operating nuclear power plants [11].

Remarkable advantages of nuclear energy over other technologies are [12]:

- Uranium has an energy density which is about 1 million times greater than traditional energy sources. In other words, one uranium pellet[3] is capable of producing the same amount of energy as 1 ton of coal.
- Around 3 million PV solar panels or over 400 utility-scale wind turbines are needed to match the same annual energy production as one conventional

[2]Nuclear reactors are divided into four different generations. In section 2.3 we find a better explanation of the different nuclear reactor generations.

[3]An uranium pellet is the fuel of a nuclear reactor. It consists of a small cylinder about 1 cm tall and 1 cm in diameter.

gigawatt-scale nuclear reactor.

- The average capacity factor[4] of nuclear reactors, with more than 90% being the highest among all the other technologies.

The global opinion on nuclear energy is gradually changing to a more pro-nuclear position. As an example, for the first time since the Fukushima Daiichi nuclear disaster in 2011, the majority of the Japanese public is in favour of nuclear energy [13]. Moreover, in 2022, more than half of the Swedes who participated in a poll about nuclear energy [14] were in favour of building new nuclear reactors if needed. We also observe an increase in pro-nuclear opinion among US citizens [15] as well.

We are currently witnessing the dawn of a new era in the nuclear energy industry, characterized by the emergence of advanced technologies like Generation IV (GenIV) reactors and Small Modular Reactors (SMRs). This thesis delves into the comprehensive investigation of a prototype for an experimental reactor belonging to this next generation of reactors. The focus of this study centers on the activation of internal structural components, aiming to assess the extent of radioactivity associated with these components and explore the feasibility of their recycling. The objectives and goals of this thesis are outlined in Section 1.1, while Section 1.2 provides a comprehensive overview of the entire thesis structure.

## 1.1 Aims and Objectives

Stiftelsen för Strategisk Forskning (SSF) or the Swedish Foundation for Strategic Research (eng.), announced the funding of 200 million SEK on future advanced technology for sustainability [16] as a national call to meet the Agenda 2030 [17]. Of the 17 different sustainability goals proposed by the UN Agenda 2030, one of the most important is the urgent action toward combating climate change. The funding was distributed between four Swedish research centres in the following areas:

1. Future nuclear power
2. Plant biotechnology, including GMO and CRISPR/Cas9
3. Hydrogen/fuel cells

[4]Capacity factor is a unitless ratio between the actual energy produced over the theoretical maximum energy output for a given period of time.

4. Next generation of antibiotics and/or actions to prevent pandemics

This thesis will be concentrated on the subject of *Future nuclear power*, which encompasses a dedicated focus on Generation IV (GenIV) reactors and Small Modular Reactors (SMRs). The research presented forms an integral part of the larger SUNRISE (Sustainable Nuclear Energy Research In Sweden) centre. SUNRISE involves collaboration among researchers from prestigious institutions such as KTH Royal Institute of Technology, Luleå University of Technology, Uppsala University, and prominent nuclear industry entities in Sweden. One significant facet of the SUNRISE project is the development of the SUNRISE-Lead-cooled fast reactor (SUNRISE-LFR), which serves as a research and demonstration reactor in Sweden, as elucidated in [18]. This thesis will focus on the following key aspects:

- Investigating the activation of structural components in SUNRISE-LFR prioritizing the steam generators.
- Special focus on novel materials such as Fe-10Cr-4Al-RE (FeCrAl)[1] and Alumina-Forming-Austenitic (AFA) stainless steels [2].
- Study the activation of the primary vessel and calculate its cooling time[5].
- Examine the amount of dose received from 1 steam generator unit.
- Determine the neutron and gamma flux received by personnel outside the reactor vessel during operation.

We aim to understand and study the previously mentioned goals through computer simulations using the Monte Carlo code Serpent 2 [19][6]. Throughout this thesis, we will refer to it as Serpent.

[5]The cooling time referred here stands for the time needed for the radiation to decay below acceptable limits.

[6]Serpent is a three-dimensional reactor physics calculation code created to simulate, by using a Monte Carlo approach, neutron-interaction physics and burnup calculations.

## 1.2 Outline

This thesis will be structured into six main chapters. The first chapter serves as the introduction, encompassing a comprehensive discussion of the latest perspectives regarding nuclear energy and the evolution towards a more pro-nuclear position. Moreover, it elucidates the numerous advantages associated with nuclear energy. This chapter also outlines the primary objectives of the thesis and provides an overview of the SUNRISE project. The second chapter delves into the theoretical background, offering a detailed account of key concepts essential for comprehending the underlying physics within a nuclear reactor. Following the background, the third chapter presents the methodology employed throughout the study. This chapter provides the data analysis techniques utilized to evaluate the results obtained from the Serpent simulations. The fourth chapter showcases the most interesting findings, accompanied by a multitude of plots and figures. The discussions o the results will be presented in the fifth chapter. Finally, the concluding chapter summarizes the key findings and highlights the significant contributions made by the research, drawing meaningful conclusions based on the gathered results and a short paragraph talking about the possible future work.

# Chapter 2

# Theoretical Background

In this chapter, we will see the crucial theoretical background to the physics involved inside a nuclear reactor and how it is possible to harvest the power of an atomic nucleus. We will discuss problems associated with using nuclear power as an energy source and how we deal with them. Furthermore, in section 2.3 we will address the new generation IV reactors, and the improvements and advantages of this new technology. Finally, in the last section, we will explore the SMR technology and why it, from an economical, time-saving and safer point of view, is the next step in the future of nuclear energy.

## 2.1 Neutron Spectrum

Most of the commercial nuclear reactors in operation worldwide are classified as thermal reactors. Thermal reactors use low-energy (thermal) neutrons to induce fission, the typical energy for thermal neutrons is around $0.025$ eV [20]. To slow the neutrons down, a moderator is employed, with water commonly utilized as a moderator in the majority of thermal-spectrum reactors. Neutrons have a probability of interacting with a heavy nucleus, and, if captured, fission might take place. For thermal neutrons, fission can only happen for certain heavy nuclei with an odd number of nucleons e.g. $^{233}$U, $^{235}$U and $^{239}$Pu [21]. In contrast, SUNRISE-LFR will make use of fast-spectrum neutrons. The fast spectrum regime defines neutrons with energies larger than 0.1 MeV.

Fig. 1 shows the fission cross-section[1] energy dependence for $^{235}$U and $^{239}$Pu. At high energies, in the fast spectrum regime, the probability of fission for $^{238}$U starts to be noticeable.

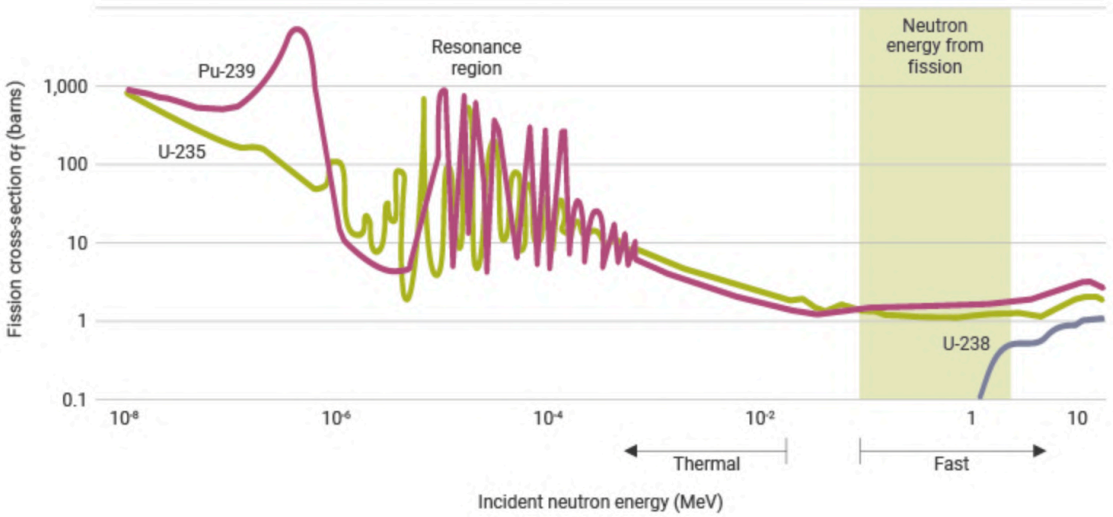


Figure 1: Neutron cross-section for $^{235}$U, $^{238}$U and $^{239}$Pu. Image taken from [21]. Source: NEA, Plutonium fuel - an assessment (1989); Taube, Plutonium - a general survey (1974).

Most nuclear reactors use the fission of $^{235}$U to generate energy. Typically, for every $^{235}$U nuclei that undergo fission around 200 MeV of energy is released [21]. Additionally, each fission event releases, on average, 2 to 3 neutrons [21]. Furthermore, the combined effect of prompt[2] and delayed[3] fission neutrons allow humans to sustain nuclear chain reactions and the faculty to harvest the power of the atomic nuclei.

## 2.2 Radioactivity form Neutron activation

A typical commercial PWR has a neutron flux in the order of $10^{13}$ to $10^{14}$ neutrons $\cdot$ cm$^{-2}$ $\cdot$ sec$^{-1}$ [22]. In contrast, fast spectrum reactors have a neutron flux in the order of $10^{15}$ to $10^{16}$ neutrons $\cdot$ cm$^{-2}$ $\cdot$ sec$^{-1}$ [20]. The high neutron flux poses challenges in terms of materials selection and reactor design. This elevated neutron flux induces substantial radiation damage, degradation of structural materials and activation of

[1]The cross-section is used to compute the probability for a nucleus to have a certain type of interaction between another nucleus or particle. Those interactions can be scattering, absorption and fission. The unit of cross section is known as *barn* which is 1 barn $= 10^{-24}$ cm$^2$.

[2]Neutrons releases during fission.

[3]Neutrons released by the daughter nuclei seconds or minutes later.

reactor components, which requires careful consideration and specialized materials capable of withstanding the harsh conditions.

One of the main objectives of this thesis is to compute the amount of activation in the internal components of the reactor. To ensure the safety of individuals and the environment, it is imperative to comprehend how a constant flux of neutrons, irradiating specific materials, can trigger radioactivity within that same materials.

Most structures inside a nuclear reactor are subjected to intense neutron irradiation. As mentioned before, a fast spectrum reactor such as SUNRISE-LFR, has a typical neutron flux in the order of $10^{15}$ to $10^{16}$ neutrons $\cdot$ cm$^{-2} \cdot$ sec$^{-1}$ [20]. Neutron activation, also known as neutron-induced radioactivity, refers to the process in which atomic nuclei capture neutrons, resulting in the creation of radioactive isotopes. This can lead to the emission of various particles or photons. Typically, an unstable nucleus might decay by emitting $\alpha$ particles (which is a nucleus of helium-4), $\beta$ particles (electrons or positrons) or $\gamma$-rays if the activated isotope is in an excited state. After the decay, the resulting nucleus can be excited as well, emitting one or multiple $\gamma$-rays.

## 2.3 On New Generation Reactors

Generation IV International Forum (GIF) initiative was created with the objective of creating a collaborative international effort to develop the research to test the feasibility and performance of fourth generation nuclear systems, with the ultimate objective of enabling their industrial implementation by the year 2030. GIF is an organization that brings together 13 countries (Argentina, Australia, Brazil, Canada, China, France, Japan, Korea, Russia, South Africa, Switzerland, the United Kingdom and the United States). Euratom also takes part in the organization and represents 27 European Union members. GIF has set four main goals that any Gen IV reactor must obey [23]:

- **Sustainability Goals**
  - Clean sustainable energy production with long-term availability of systems and effective fuel utilization.
  - Minimization and management of nuclear waste and reducing the long-

term stewardship burden while improving public health and environment protection.

- **Proliferation Resistance and Physical Protection Goals**
  - Making nuclear waste material from generation IV reactors the least desirable way for diversion or theft of weapons-usable material.
- **Economics Goals**
  - Clear life-cycle cost advantage over other energy sources.
  - Level of financial risk compatible with other energy systems and projects.
- **Safety and Reliability Goals**
  - Exceptional safe and reliable systems.
  - Very low probability of reactor damage
  - Elimination of the need for offsite emergency response.

GIF has proposed **six** nuclear reactor technologies as the most probable new Gen IV reactors. The chosen designs are the gas-cooled fast reactor (GFR), the lead-cooled fast reactor (LFR), the molten salt reactor (MSR), the sodium-cooled fast reactor (SFR), the supercritical-water-cooled reactor (SCWR) and the very high-temperature reactor (VHTR). Every single type of reactor deserves a whole thesis of its own. In this case, we will only focus on a lead-cooled fast reactor since the SUNRISE-LFR is exactly this type of reactor.

Lead-cooled fast reactors have significant advantages over conventional light-water reactors (LWRs). LWRs use water as a coolant due to its simplicity, abundance and cheap price. The main problem with water is the low boiling temperature, 100°C at atmospheric pressure. For LWRs to convert the heat into electricity more efficiently they need to increase their internal pressure to increase the boiling point of water. For a pressurized water reactor (PWR), the internal pressure can reach 15 MPa (150 times the atmospheric pressure) which elevates the boiling point of water to above 300°C. At a pressure of 15 MPa, the reactor vessel needs a wall thickness of approximately 200 mm [24]. In contrast, lead has a very high boiling point at atmospheric pressure (1749 °C) allowing the reactor to operate at higher temperatures, therefore increasing the thermodynamic efficiency. In the case of the SUNRISE-LFR, the high boiling

point of lead allows the reactor to operate at approximately atmospheric pressure, thus decreasing the wall thickness to 40 mm [18]. Additionally, the SUNRISE reactor will operate with coolant temperatures from 420°C at the inlet of the core to 550°C at the outlet of the core [18].

One of the main advantages of fast-spectrum metal-cooled reactors is their ability to breed. Breeding is the process of transmuting fertile material such as $^{238}$U to fissile material, in this case, $^{239}$Pu. The following reaction shows how breeding occurs in a breeder reactor fuelled with uranium:

$$^{238}\mathrm{U} + {}^{1}\mathrm{n}, \rightarrow {}^{239}\mathrm{U} \rightarrow {}^{239}\mathrm{Np} + \beta^{-} + \bar{\nu} \rightarrow {}^{239}\mathrm{Pu} + \beta^{-} + \bar{\nu}. \tag{2.1}$$

$^{238}$U is however not the only nuclide that can exhibit breeding. It is possible to breed from other fertile sources. The following process shows how it is also possible to breed $^{233}$U (which is fissile) from $^{232}$Th:

$$^{232}\mathrm{Th} + {}^{1}\mathrm{n} \rightarrow {}^{233}\mathrm{Th} \rightarrow {}^{233}\mathrm{Pa} + \beta^{-} + \bar{\nu} \rightarrow {}^{233}\mathrm{U} + \beta^{-} + \bar{\nu}. \tag{2.2}$$

The ability to breed allows the reactor to ”create” new fuel, extending the fuel life. SUNRISE-LFR will work with the same fuel for approximately 16 years [18].

## 2.4 The Advantages of Small Modular Reactors

Nowadays, modern large-scale nuclear reactors can produce more than 1 GWe of power. Accomplishing such high power output entails the utilization of large reactor vessels. The manufacturing of the reactor vessel holds significant importance in terms of the economic viability and time required for a nuclear reactor plant to commence operations. Given their considerable size, nuclear reactor vessels necessitate extensive welding, which is a laborious and costly human-driven process. As a result, the nuclear industry is transitioning towards a more economically viable, faster and safer alternative.

According to IAEA [25], a Small Modular Reactor (SMR) is defined as a nuclear reactor with an electrical power output of up to 300 MW electric. One of the many benefits of reducing the size of the units is the ability to optimize the process of building the whole nuclear reactor, enabling the construction of nuclear power plants

to be faster and cheaper. SMRs reduce the risk of financial failure since the initial capital investment is greatly reduced. Furthermore, the reduction in the size of the nuclear core facilitates the implementation of passive safety systems with greater ease. Additionally, in case of a severe accident, if the reactor core is exposed to the environment, the source term[4] associated with SMRs is considerably smaller than a conventional gigawatt scale LWR.

[4]The source term is the magnitude and mix of the radionuclides released from the core during a severe accident.

# Chapter 3

# Methodology

Within this chapter, the SUNRISE-LFR reactor's design will be provided, along with an exploration of the methodology employed to accurately compute the activation levels within its structural components. Notably, a comprehensive description of the various structural materials implemented in the reactor, such as the Fe-10Cr-4Al-RE (FeCrAl) [1] and alumina-forming-austenitic (AFA) stainless steels [2], will be presented. Emphasis will be placed on the steam generators, alongside an explication of the approach employed for dose computation from a single unit. Lastly, the method utilized for calculating the neutron and high-energy photon flux outside of the reactor will be presented. The majority of geometric designs and activity calculations have been executed employing the Monte Carlo simulation code Serpent.

## 3.1 Design of SUNRISE-LFR

The design of the SUNRISE reactor employed in this thesis closely emulates the reactor configuration presented in [18]. The reactor core comprises 54 fuel assemblies, with each assembly housing 217 fuel rods. The fuel material is 12 at.% $^{235}$U enriched uranium nitride. Surrounding the fuel assemblies are 60 reflector assemblies, employing zirconium dioxide as the pellet material. Within the core, there are evenly distributed arrangements of 2 reactivity control assemblies and 4 shut-down control assemblies. The central assembly in the core remains unoccupied to promote a more uniform neutron flux distribution and to potentially facilitate experiments. The core layout can be found in Fig.2.

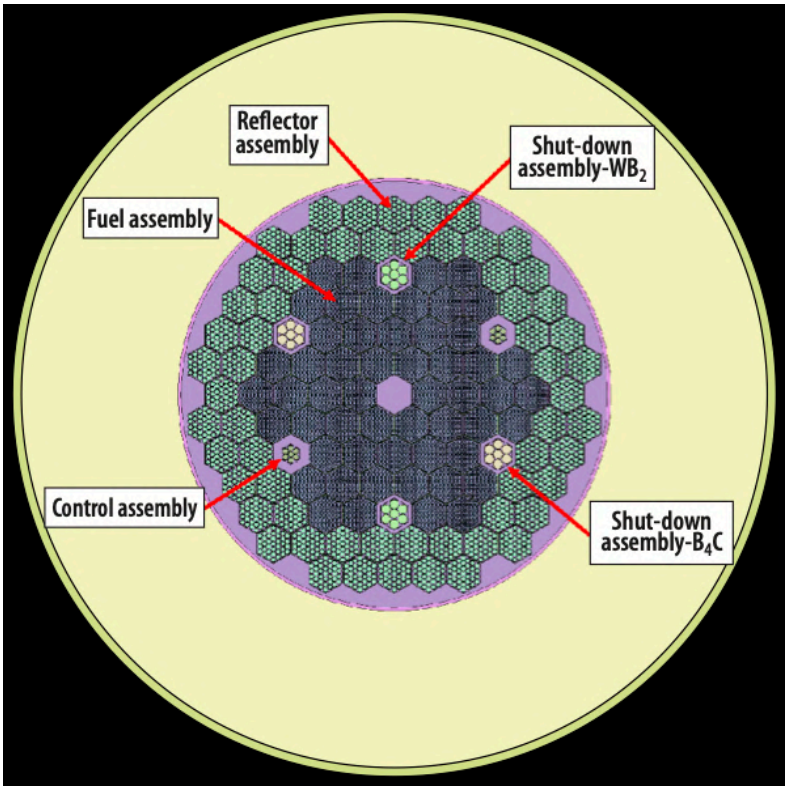


Figure 2: Core layout of the SUNRISE-LFR. Control and shut-down rods are inserted.

The primary focus of this thesis revolves around the assessment of the activation of structural components of the reactor. Situated at the top and bottom of the SUNRISE-LFR core are the respective support grids, with the bottom grid,
exhibiting a greater thickness compared to the top grid in order to support the core. Around the core, we can find the reactor core barrel, which serves as a separation between the hot leg and the cold leg. These structural components predominantly employ FeCrAl as their bulk
material. The reactor vessel is primarily constructed using SS316L stainless steel with an overlay of AFA. The reason behind incorporating AFA as an overlay lies in its capacity to endure lead corrosion while

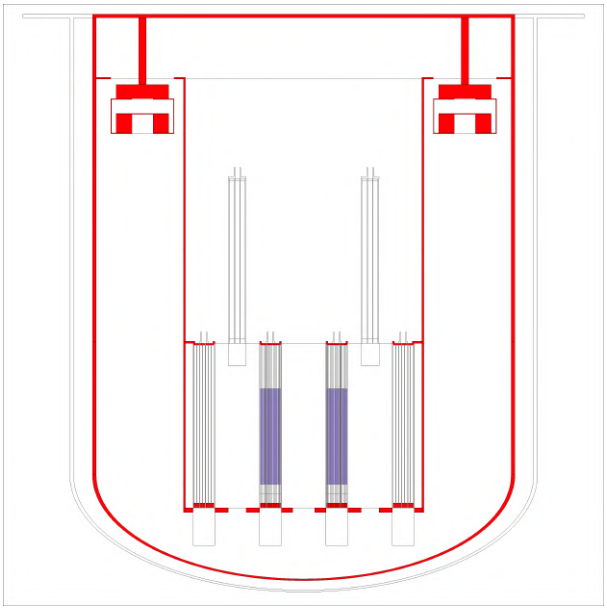

Figure 3: Vertical cross-section of the SUNRISE-LFR. The red parts highlight the studied structures in this thesis. Control and shut-down rods are extracted.

effectively welding to the vessel. This choice is made because FeCrAl exhibits poor weldability with the reactor vessel. The primary vessel is designed with a wall thickness of 40 mm, while the AFA weld overlay, relevant to this thesis, is implemented with a thickness of 200 microns. A vertical cross-section of the SUNRISE-LFR reactor can be found in Fig.3.

The investigation conducted places significant emphasis on the examination of the activation of the steam generator modules. The reason for studying the activation of these modules lies in assessing the feasibility of their recycling and determining the level of radiation associated with handling them by actual personnel. The modules are located on the top portion of the core barrel, which exhibits 12 evenly distributed apertures encircling the reactor. Out of these openings, 10 are allocated for the placement of steam generators, while the remaining two are designated for dip coolers. Each steam generator is comprised of multiple sections, including the pump shaft, pump box, and walls, all manufactured from FeCrAl material. Lastly, the heat exchange will take place between 11 spiral tubes filled with water and steam, stacked one upon another, and the liquid lead. The compound tubes will have an outer layer made out of FeCrAl and an inner layer composed of A800 stainless steel. A vertical cross-section of the steam generator design can be found in Fig.4.

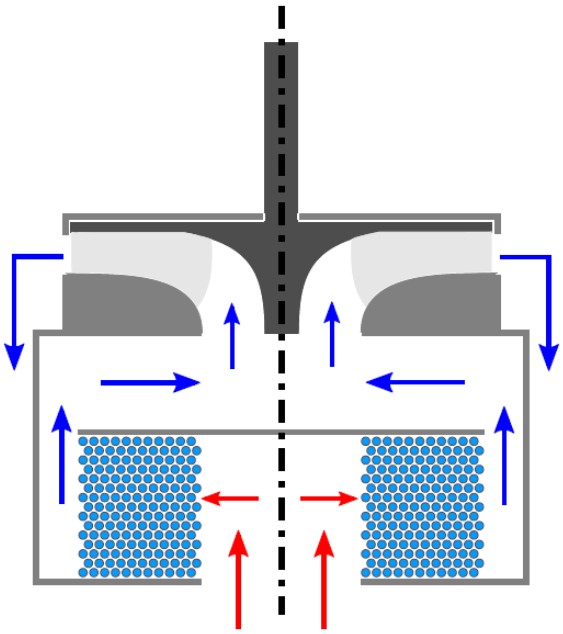

Figure 4: Vertical cross-section of the stem generator unit. Located in the top part of the reactor in Fig.3. Image taken from [18].

## 3.2 Dose Calculations

The dose calculations for this study are divided into two subsections. Firstly, the dose received as a consequence of neutron activation in the structural components, reactor vessel and steam generator modules, and secondly, the dose received by

personnel located outside the reactor. In the former case, we will assess the specific external gamma and x-ray dose rate, ingestion, and inhalation radiotoxicity of various structural components, with particular focus on FeCrAl and AFA. Additionally, we will analyze the overall external dose rate originating from a single steam generator module. In the latter case, we will investigate the neutron and gamma-ray flux per square centimetre that an individual may be exposed to when positioned immediately outside the reactor vessel, without any form of protection. Naturally, in practical applications, multiple layers of protection, such as concrete and neutron absorbent coatings, will be incorporated around the reactor to minimize the escaping radiation. Moreover, we will examine the neutron and gamma flux on top of the reactor. It is important to underscore that the reactor employs lead as a coolant, providing optimal shielding against gamma rays.

### 3.2.1 Internal Structural Components, Reactor Vessel and Steam Generators

The Monte Carlo code Serpent 2, operates based on input files that define the geometry of the reactor. The resulting geometry visualization is depicted in Figure 3. Beyond the geometry specification, various other parameters can be defined. Serpent is specifically designed for neutron transport calculations, later versions added the capability of simulating photon transport calculations as well, enabling the execution of simulations encompassing a wide range of scenarios. In this particular study, we conducted a burn-up calculation on the structural materials, to see their depletion, while assuming a constant initial fuel composition. The simulation was conducted assuming continuous operation of the reactor for 16 years, representing the worst-case scenario, while acknowledging that the actual reactor would have periodic shutdowns for fuel reshuffling, replacement of experiment samples, inspections and maintenance. In the case of the steam generator modules, the burn-up simulation time amounted to approximately 1.5 years, as these components are planned to be replaced yearly.

After conducting the aforementioned simulations, Serpent generated an output file containing a comprehensive set of parameters for all the radioactive isotopes present in the materials of interest. Of particular significance for this study were the activity, ingestion and inhalation toxicity associated with each isotope. Additionally, the volume and density of each structural component were provided to facilitate further

analysis. Subsequently, we proceeded to simulate the decay of these isotopes over a span of 10 000 years, in order to evaluate the potential for recycling and quantify how much radioactive waste is produced. The resultant output file provides a detailed representation of the decay evolution of the concentration of these isotopes.

Among all possible isotopes simulated, our focus was primarily on those capable of posing significant risks to human health. Initially, we selected only those isotopes with a specific activity surpassing the regulatory limit set in [3]. To identify the isotopes exceeding this limit, we utilized the activity values obtained from the Serpent simulations. The activity is measured in Becquerels (Bq) or disintegrations per second. To determine the specific activity a (Bq/g), we divided the activity $A$ by the product of the material's volume $V_{\text{material}}$ (in $\text{cm}^3$) and its density $\rho_{\text{material}}$ in ($\text{g}/\text{cm}^3$):

$$\text{a} = \left[\frac{\text{Bq}}{\text{g}}\right] = \frac{A}{V_{\text{material}} \cdot \rho_{\text{material}}}. \tag{3.1}$$

One can observe that certain isotopes exhibit short half-lives. An example of such a short half-life is aluminium-28, which possesses a half-life of $2.245$ minutes [26]. These short-lived nuclei are not typically encountered in the clearance limit[1] [3], but they will also be presented in this thesis since it can be interesting to see their contribution to the total dose. However, quantifying the potential radiation exposure associated with handling these activated materials requires more than just the specific activity. To derive the "specific external gamma and x-ray dose rate" $d$, we can utilize the "Specific Gamma-Ray Dose Constants" documented in [27]. The specific gamma-ray dose constant $\gamma$ (expressed in $\text{mSv} \cdot \text{h}^{-1} \cdot \text{MBq}^{-1}$), indicates the effective full-body gamma radiation dose rate resulting from a point source of a specific nuclide located at a distance of 1 meter. To approximate the behaviour of a point source, we divide the specific gamma-ray dose constant by the total mass of the source, obtained through its volume and density. This approach enables us to calculate the specific external gamma and x-ray dose rate, yielding results that are more representative of reality, as one gram of the material would exhibit less self-shielding. Self-shielding is the inherent characteristic of materials to stop the emission of particles from radionuclides inside

[1]The clearance limits or levels refer to the permissible level of radioactive contamination or radiation exposure that is considered acceptable for the clearance or release of a material or area from regulatory control.

the material to the surrounding environment by interactions with their internal atoms. The final specific external dose rate $d$ is expressed in $\mathrm{mSv} \cdot \mathrm{h}^{-1} \cdot \mathrm{g}^{-1}$.

$$d = \left[\frac{\mathrm{mSv}}{\mathrm{h} \cdot \mathrm{g}}\right] = \frac{\gamma \cdot A}{V_{\text{material}} \cdot \rho_{\text{material}}} = \frac{\frac{\mathrm{mSv}}{\mathrm{MBq \cdot h}} \cdot \mathrm{Bq}}{\mathrm{cm}^3 \cdot \frac{\mathrm{g}}{\mathrm{cm}^3} \cdot 10^6}. \tag{3.2}$$

### 3.2.2 Flux received by Personnel

Ensuring personnel safety during the operation of the SUNRISE reactor is crucial for the SUNRISE project. To study and evaluate the possible harms of neutron or photons leakage, we utilized the detector capabilities of Serpent. In order to simplify the analysis, we categorized the dose into two categories: neutrons and photons. To assess the worst-case scenario, where no additional protection is provided apart from the guard vessel, we positioned a detector approximately half a meter away from it. Additionally, a detector was placed in the top part of the reactor. These detector locations were selected to capture the maximum potential exposure in terms of dose for personnel.

By employing this approach, we aim to comprehensively evaluate the flux distribution, considering both neutrons and photons, with the primary focus on quantifying the potential radiation hazards in the absence of additional shielding measures.

#### Neutron leakage

In this particular case, we configured the detectors in Serpent to detect neutrons of varying energy ranges. To achieve meaningful results, we established energy bins with equal lethargy lengths rather than equal energy lengths. Utilizing energy bins with the same energy width could be misleading, as the low-energy bins would exhibit lower resolution in capturing the neutron distribution compared to the high-energy bins. By employing lethargy bins, we ensure a logarithmic spacing between the energy bins, which provides a more appropriate representation of the neutron distribution [28].

The idea is to generate a plot depicting the normalized energy-integrated neutron flux per square centimetre as a function of energy. This approach allows for a

comprehensive analysis of the neutron flux distribution while taking into account the varying energy levels across the spectrum.

To normalize the neutron flux detected outside the reactor, it is essential to comprehend the results obtained from the Serpent simulations. The detectors measure the proportion of neutrons present within a specific volume and energy range. By configuring the neutron source to emit a rate of 1 neutron per second, we can ascertain the fraction of a single neutron that will be detected within that same spatial and energy region. Multiplying this fraction by the total number of fission neutrons emitted per second enables the determination of the overall count of detected neutrons. The computation of the total number of fission neutrons generated per second relies on several key factors. Primarily, the thermal power output of the core must be determined. In the case of the SUNRISE-LFR, it is designed to produce a thermal energy output of 80 MW [18]. Furthermore, Serpent provides essential information such as the average energy produced per fission event and the fission neutron yield denoted as $\bar{\nu}$. The average fission neutron yield is the average amount of neutrons produced in a fission reaction. Utilizing these data, it becomes straightforward to calculate the number of fission events occurring per second inside the reactor.

$$\frac{80 \text{ MW}}{1.6022 \cdot 10^{-19} \text{ J/eV}} \cdot \frac{1}{\bar{\text{E}}_{\text{fiss}}} \cdot \bar{\nu} = 6.11 \cdot 10^{18} \ \frac{\text{fission neutrons}}{\text{second}}, \tag{3.3}$$

where the value calculated by Serpent for $\bar{\text{E}}_{\text{fiss}}$ is $202.78$ MeV and for $\bar{\nu}$ is $2.48$ neutrons per fission.

### Photon leakage

As previously discussed, lead is known to be an effective shielding material for gamma photons, with most gamma rays attenuated by less than half a meter of lead. The idea for the detection of gamma and x-ray photons is similar to the one mentioned for the neutrons with the detectors set in the same configuration.

# Chapter 4

# Results

This chapter will be divided into 4 sections. We will see the results obtained during the numerous Serpent simulations, focusing on the activation of structural materials, activation of the reactor vessel, activation of the steam generator units and the neutron and photon flux outside the reactor vessel. The first section examines the activation of important structural components, with particular emphasis on the critical role played by the activation of FeCrAl in these structures. In the second section, our attention shifts to the activation of the primary vessel and the role of activated AFA, which serves as an overlay for the vessel's internal part, providing corrosion protection against lead. The third section investigates the external dose resulting from a single steam generator unit after 1.5 years of irradiation. The results of the specific activity of the aforementioned sections will be compared with the clearance limit prescribed by the Swedish regulatory authority [3]. Furthermore, we will analyze the specific external dose rate, expressed in $\mathrm{mSv} \cdot \mathrm{h}^{-1} \cdot \mathrm{g}^{-1}$, as well as the dose incurred through inhalation and ingestion of one gram of activated material. Lastly, we will assess the neutron and gamma flux absorbed by an individual situated next to the reactor and on top of it.

## 4.1 Internal Structures of the Reactor - FeCrAl

This section will be divided into two distinct subsections. The first subsection will focus on the determination of the specific external gamma and x-ray dose rates, as well as the specific radiotoxicity associated with ingestion and inhalation, for each individual internal structure within the reactor. In the second subsection, the analysis will revolve around the specific activity levels of those radioisotopes exceeding the established limit

specified in [3].

The primary focus of this section pertains to the study of FeCrAl as the predominant material within all the internal structures presented in this section. Consequently, our investigation aims to show the radiological impact of the activated isotopes of FeCrAl.

### 4.1.1 Internal Structures - General Results

The results are shown from Figure 5 to Figure 13 and are displayed according to the following configuration. Each figure is divided into four subfigures. The initial subfigure, situated in the top-left position, indicates the specific section of the reactor under observation, highlighted in red. The top-right plot exhibits the specific external gamma and x-ray dose rates. The two plots in the bottom section depict the inhalation (bottom-left) and ingestion (bottom-right) radiotoxicity. Both axes in all plots utilize a logarithmic scale.

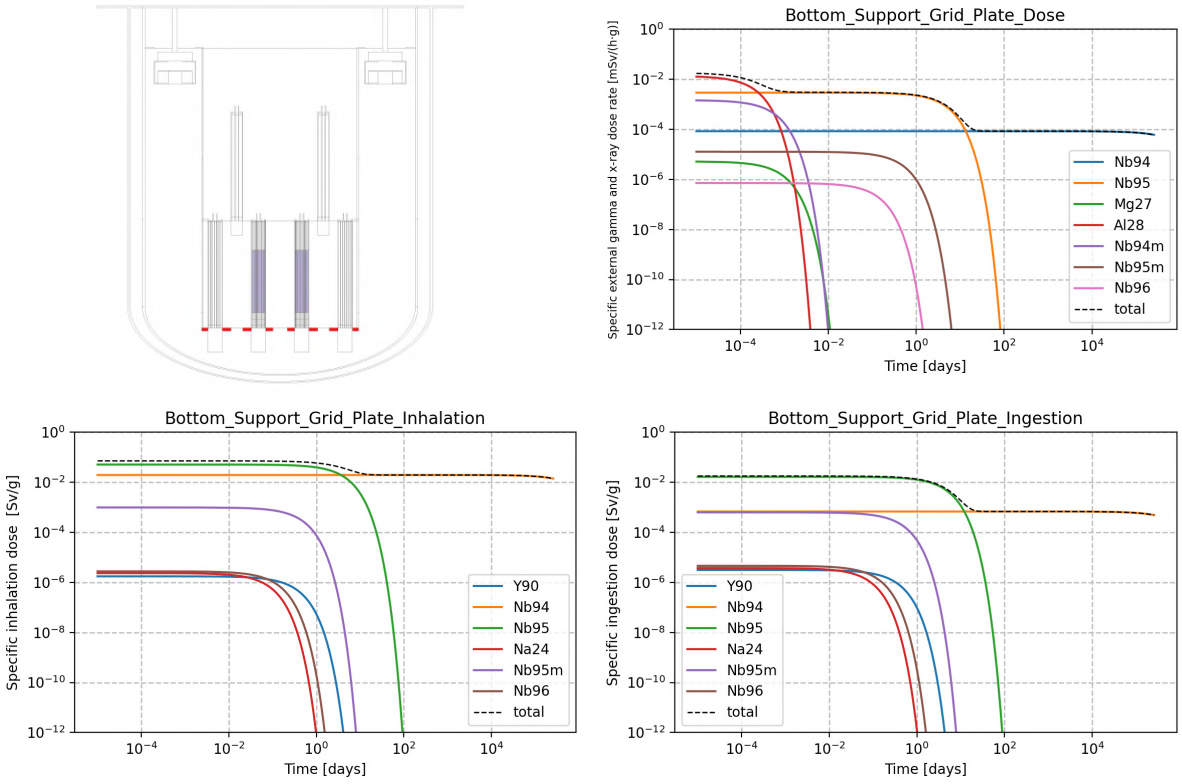


Figure 5: Results for the support grid plate.

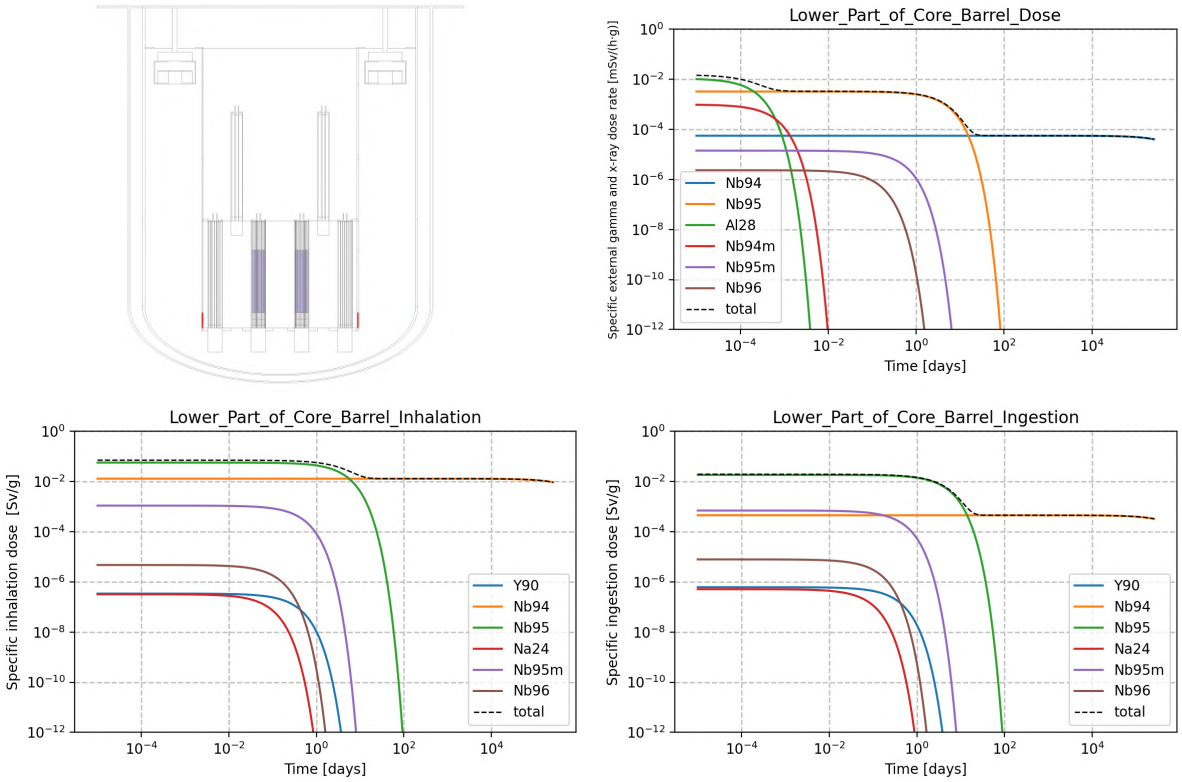


Figure 6: Results for the lower part of the core barrel.

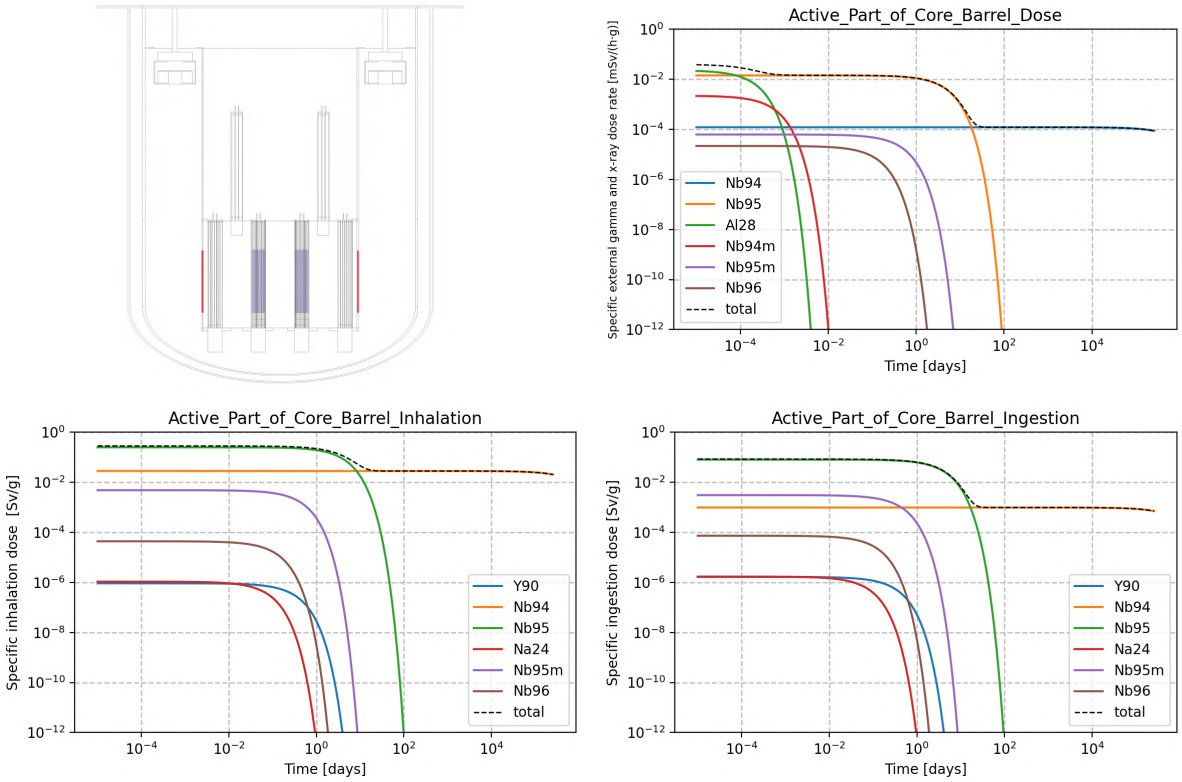


Figure 7: Results for the active part of the core barrel.

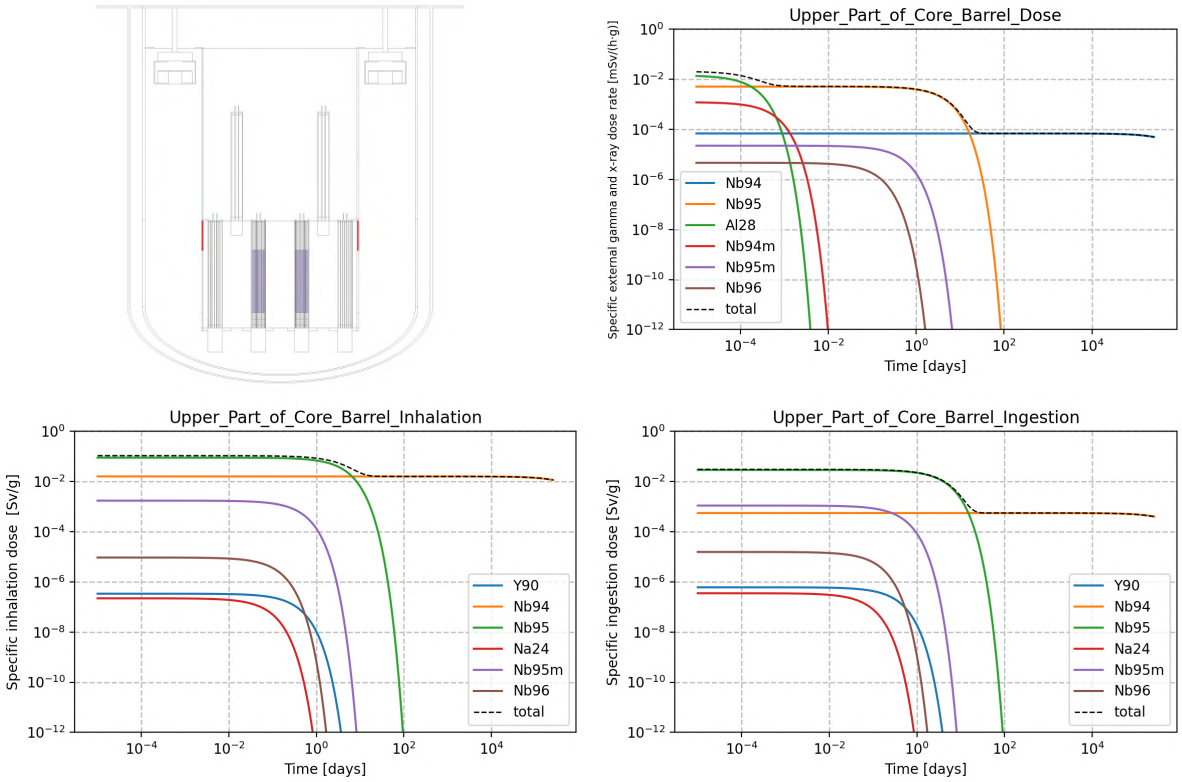


Figure 8: Results for the upper core part of the core barrel.

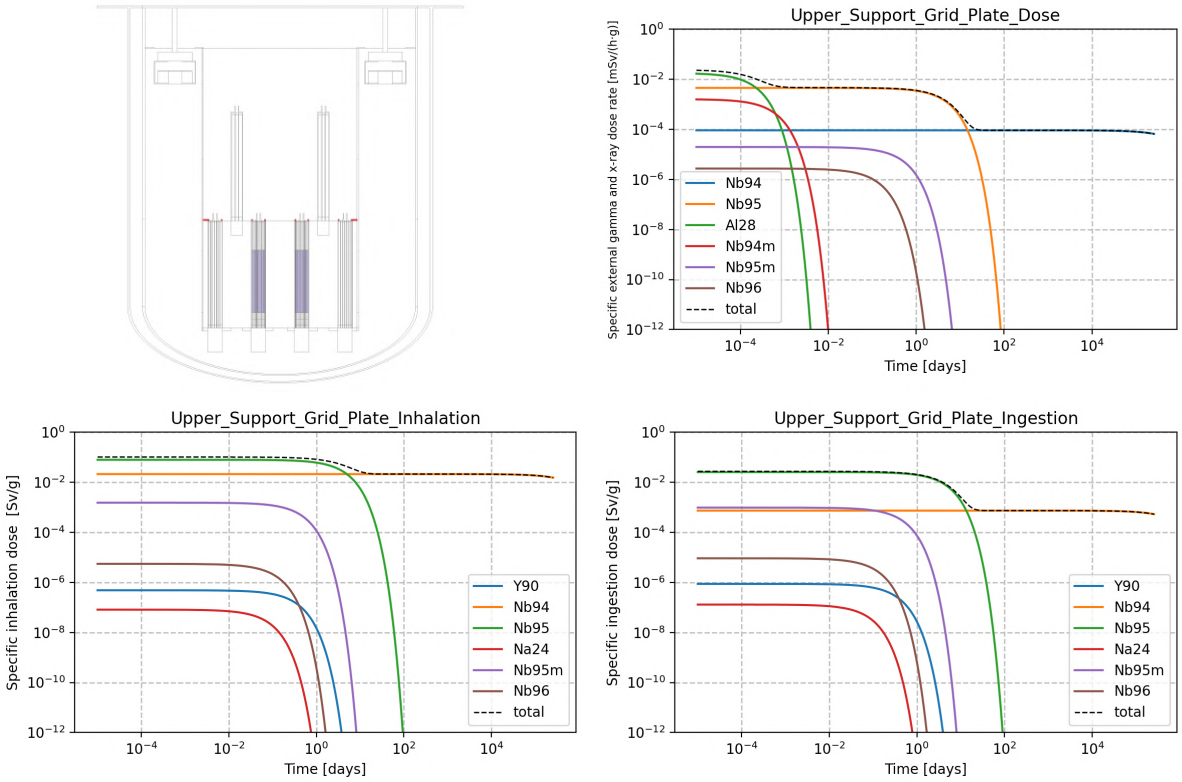


Figure 9: Results for the top grid plate.

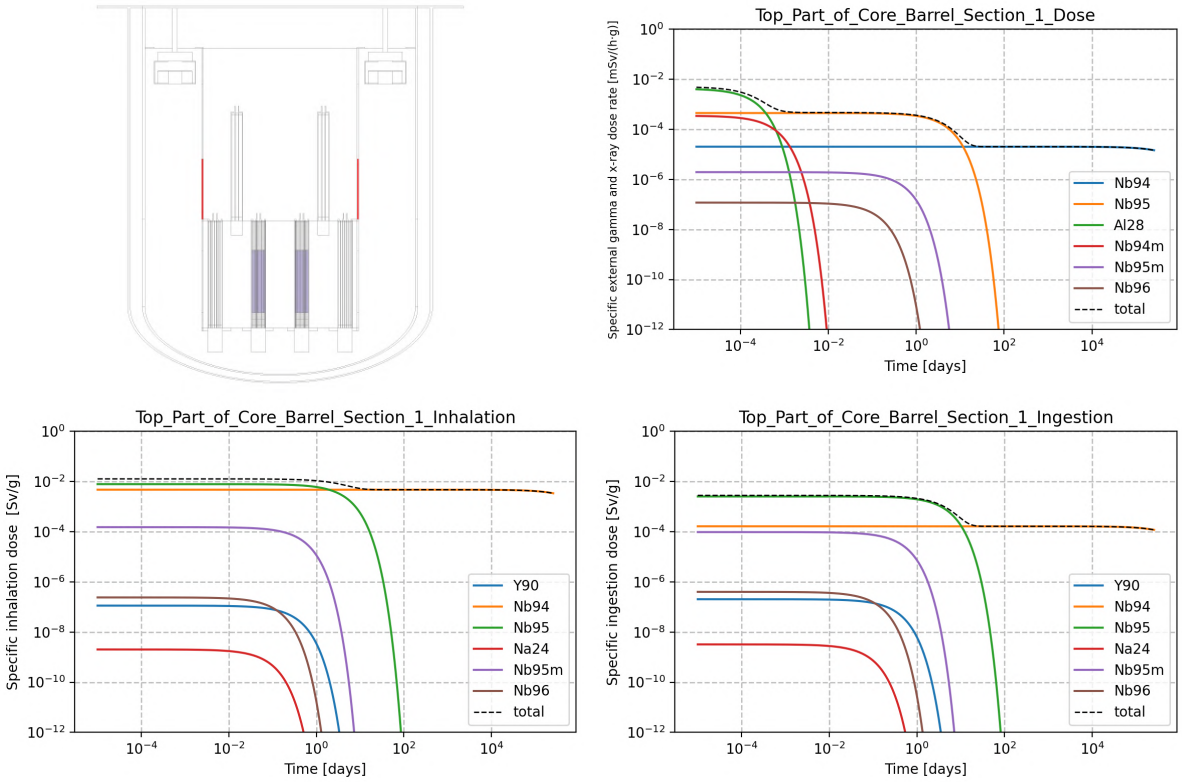


Figure 10: Results for the first section of the top part of the core barrel.

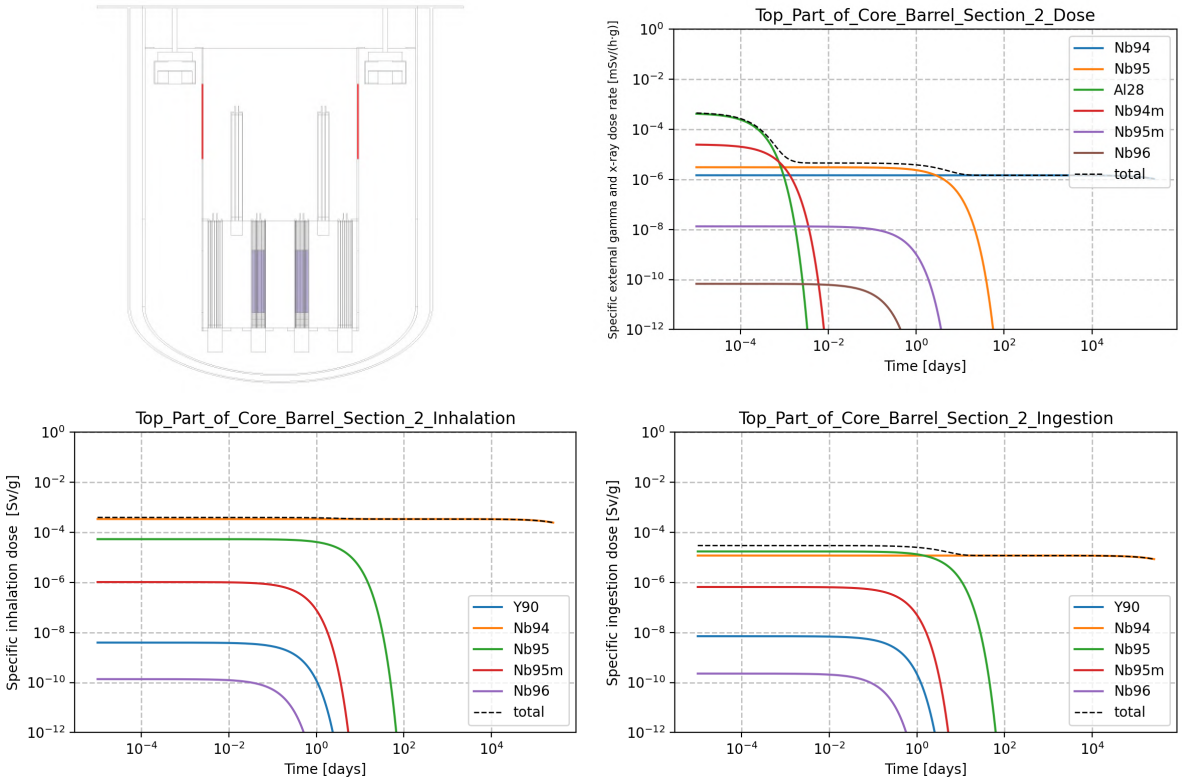


Figure 11: Results for the second section of the top part of the core barrel.

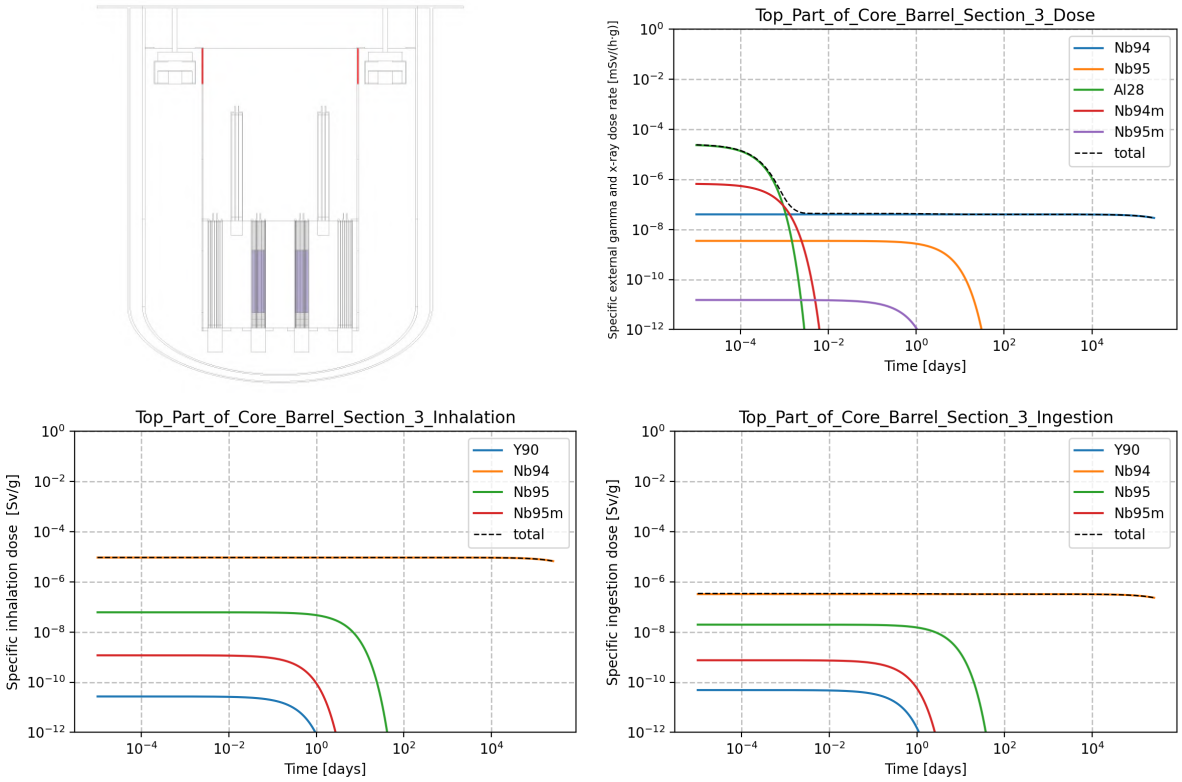


Figure 12: Results for the third section of the top part of the core barrel.

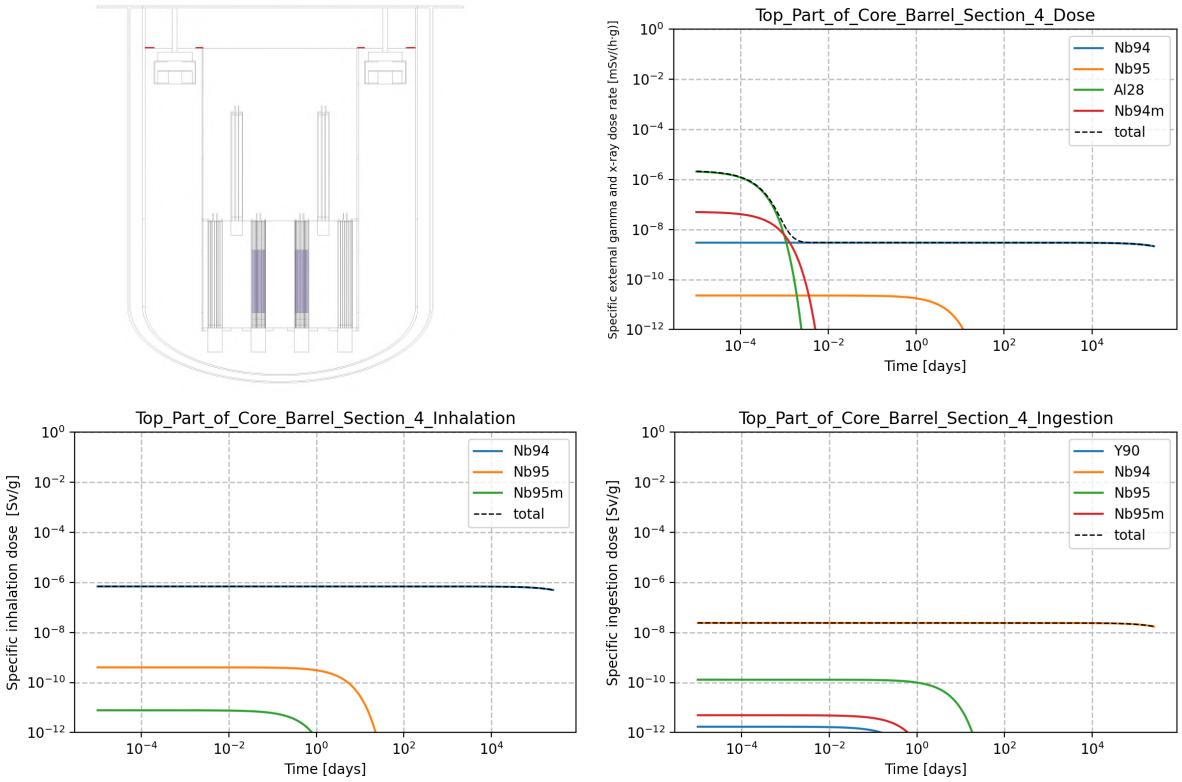


Figure 13: Results for the fourth section of the top part of the core barrel.

A proper discussion of the results will be presented in section 5. However, preliminary deduction from these results (from Figure 5 to Figure 13) shows the influence of niobium on the FeCrAl-based materials. Notably, the dominating radioisotope of niobium, namely niobium-94 (Nb94), significantly governs both the external dose and the doses incurred through ingestion and inhalation for thousands of years. In contrast, the other dominating isotopes decay within 100 days.

### 4.1.2 Internal Structures - Clearance limit comparison

In this section, Figures 14 to 22 show those isotopes with specific activities exceeding the threshold stipulated in the clearance limit document [3]. It is crucial to bear in mind that the clearance limit is different for each isotope, though only one limit is displayed as a red dashed line in the plots. This particular limit pertains to niobium-94, chosen due to its substantially longer half-life compared to other isotopes. Additionally, certain isotopes, such as aluminium-28, are absent from the clearance limit list. Therefore, The total line (represented by a black dashed line) shows an initial higher activity that quickly converges once the short-lived nuclides (such as aluminium-28) have decayed.

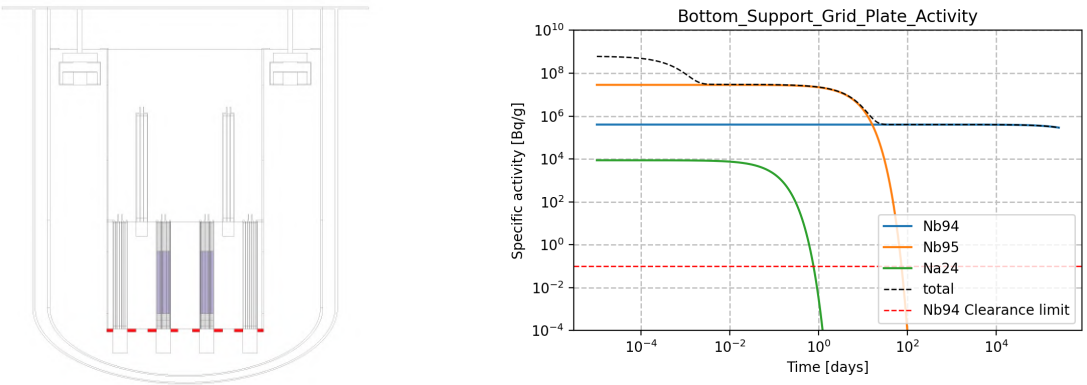


Figure 14: Results for the specific activity of the support grid plate.

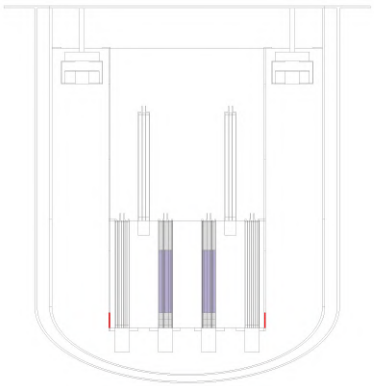

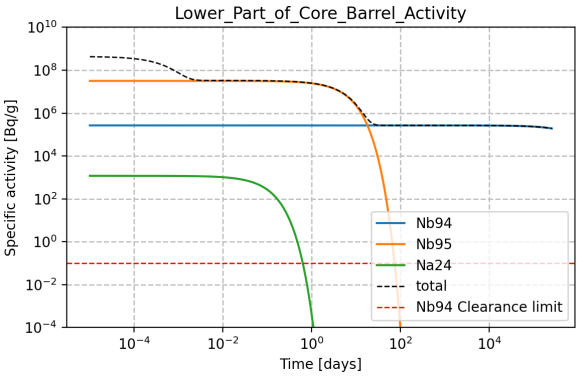


Figure 15: Results for the specific activity of the lower part of the core barrel.

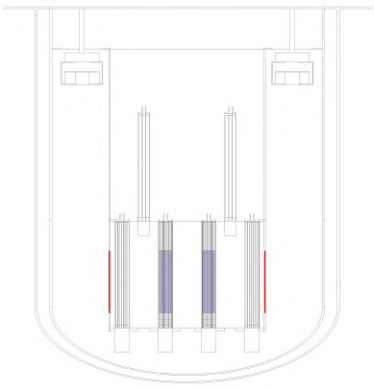

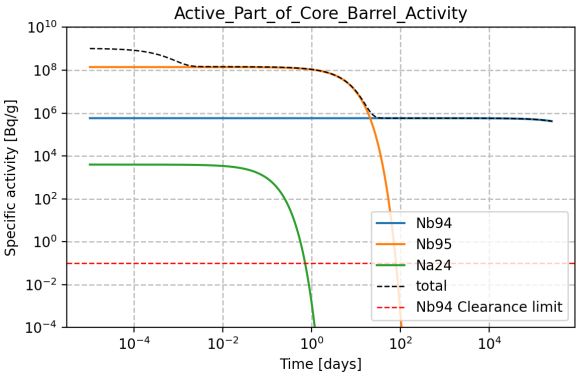


Figure 16: Results for the specific activity of the active part of the core barrel.

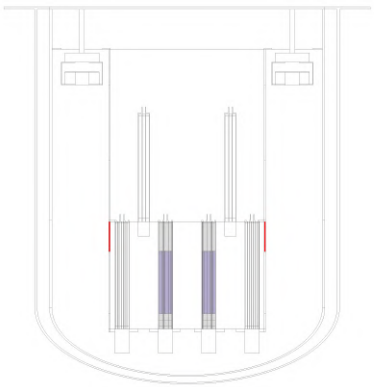

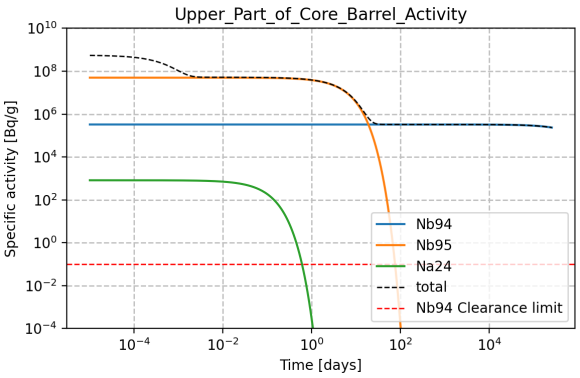


Figure 17: Results for the specific activity of the upper core part of the core barrel.

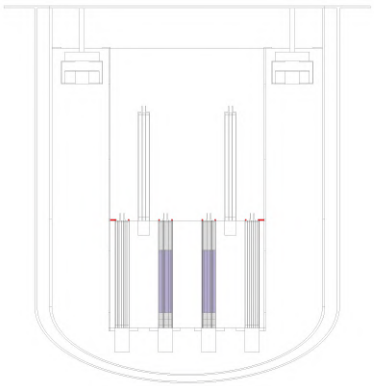

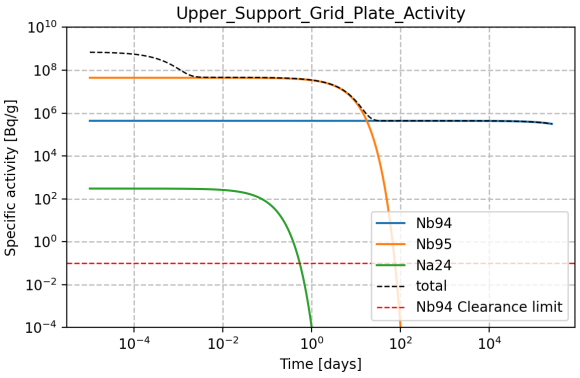


Figure 18: Results for the specific activity of the top grid plate.

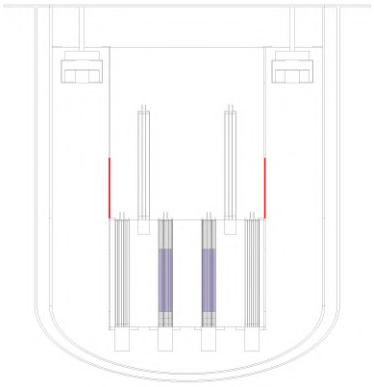

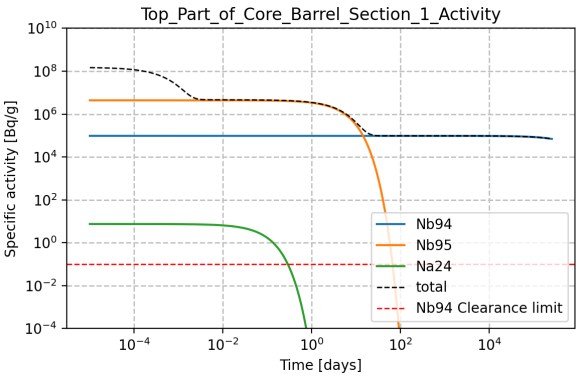


Figure 19: Results for the specific activity of the first section of the top part of the core barrel.

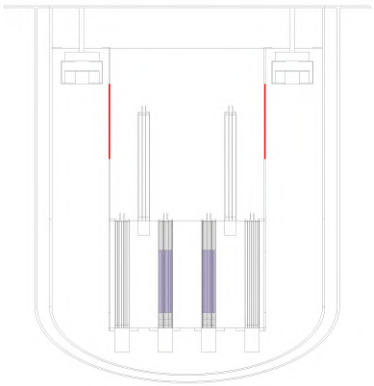

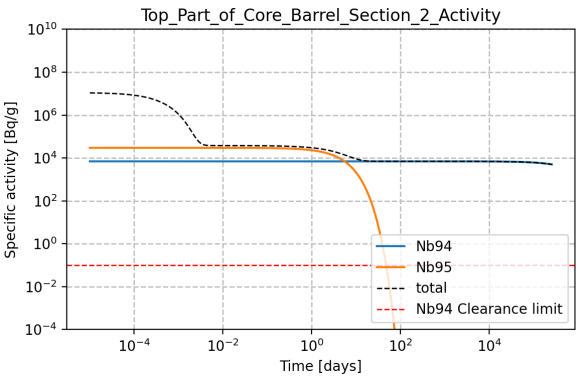


Figure 20: Results for the specific activity of the second section of the top part of the core barrel.

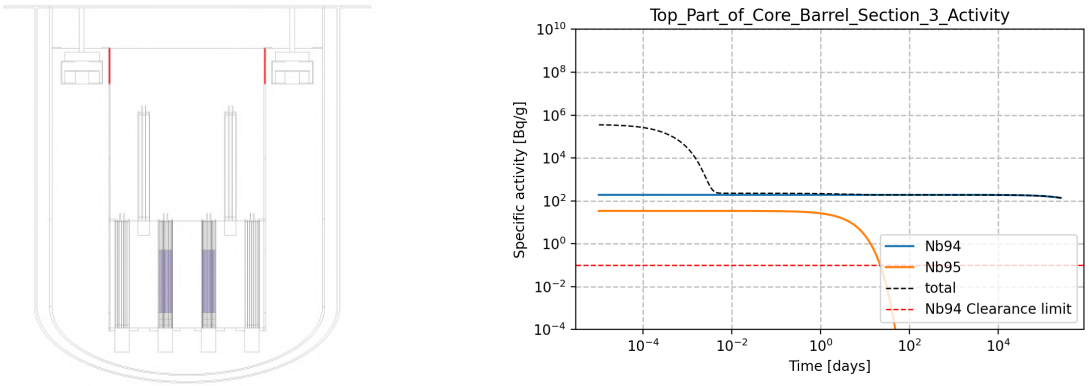


Figure 21: Results for the specific activity of the third section of the top part of the core barrel.

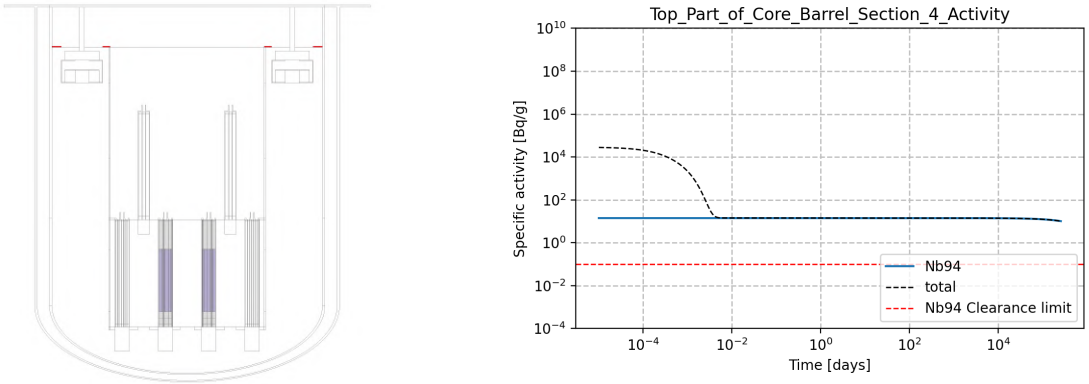


Figure 22: Results for the specific activity of the fourth section of the top part of the core barrel.

As depicted in Figures 14 through 22, we see the same trend as in the section before. The presence of niobium-94, characterized by its large half-life, engenders a scenario wherein all constituents composed of FeCrAl exceed established safety thresholds in relation to the specific activity.

## 4.2 Reactor Vessel - AFA

In this section, we will follow the same division as in the previous section. But, focusing on the activation of the AFA stainless steel. It is important to recall that our assumptions consider a 200-micron overlay of AFA onto the primary reactor vessel, which is constructed from SS316L stainless steel. Given the novelty of AFA as a material, we have also conducted an examination of its activation in the end caps employed at the top and bottom of the fuel and reflector rods. Although the AFA used in

these end caps does not serve as a structural material it can provide useful information on the activation of this material.

### 4.2.1 Reactor Vessel - General Results

The results obtained in Figures 23, 24, 25, 26 and 27 pertaining to the reactor vessel show the same distribution as in section 4.1. The upper-left image shows the part of the reactor vessel studied. The top-right plot shows the specific external gamma and x-ray dose rate. Finally, the lower plots, situated in the bottom-left and bottom-right quadrants, respectively, show the inhalation and ingestion radiotoxicity.

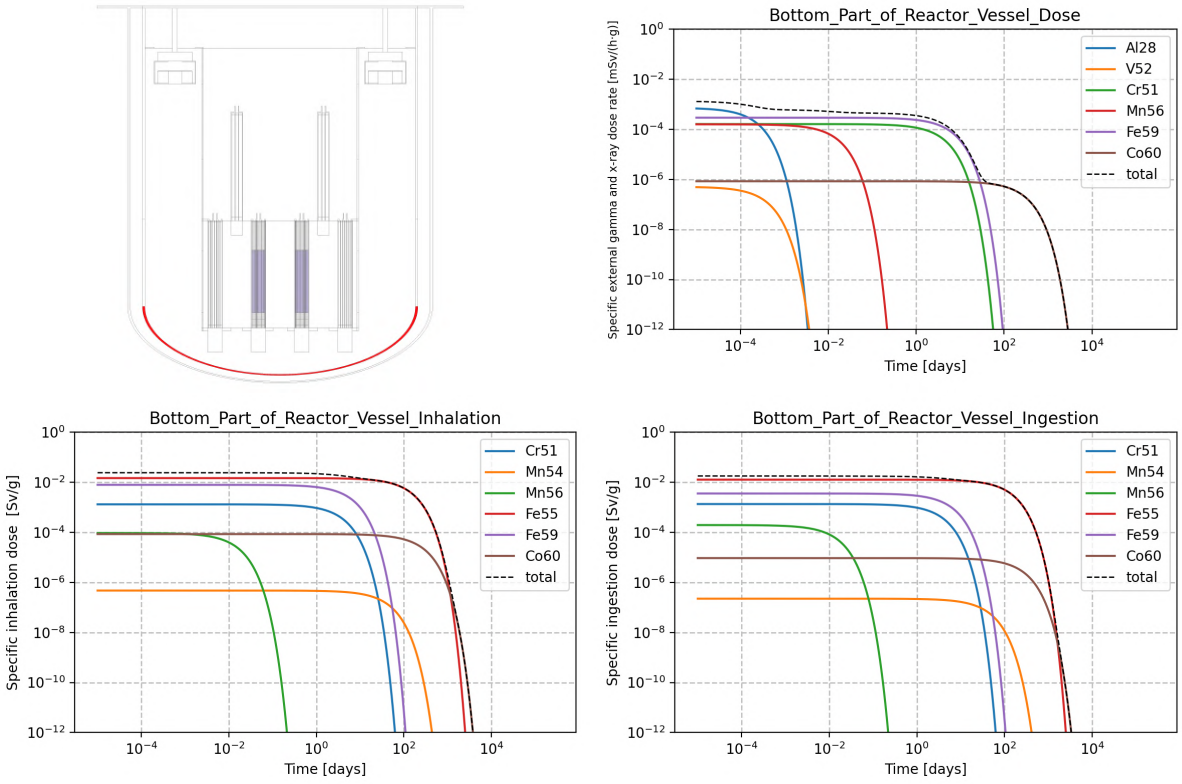


Figure 23: Results for the bottom of the reactor vessel.

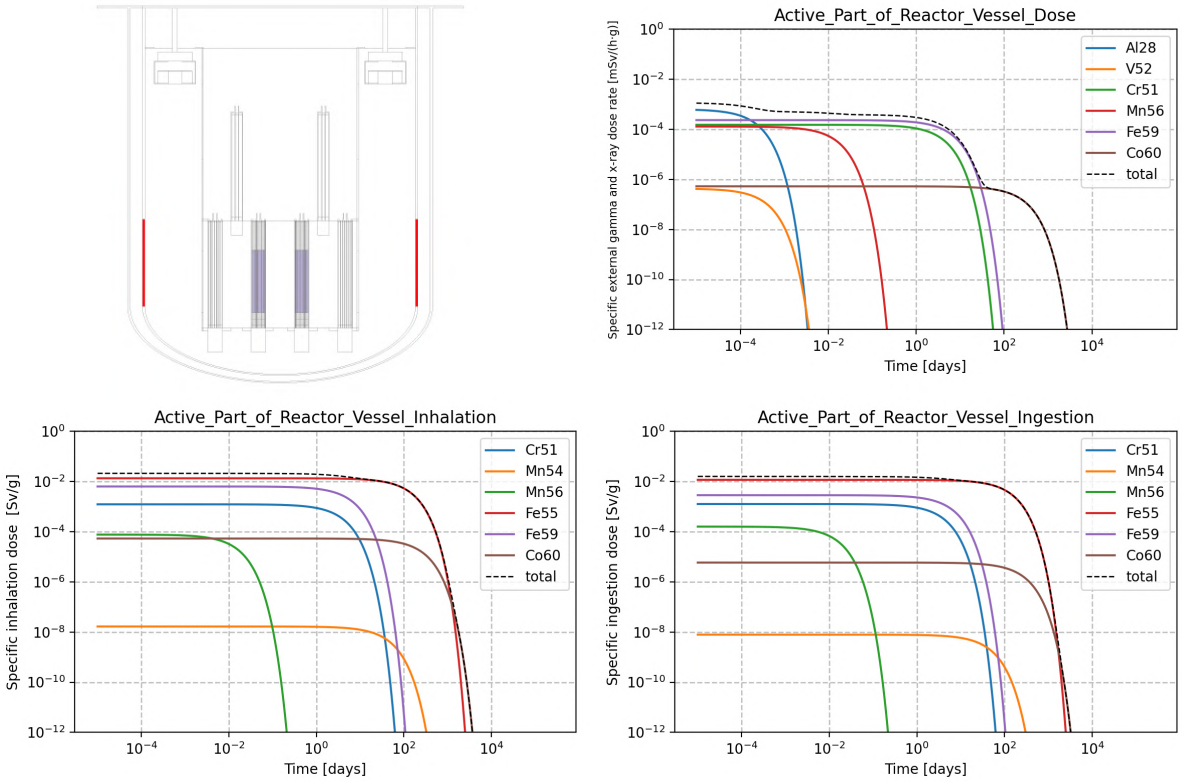


Figure 24: Results for the center of the reactor vessel.

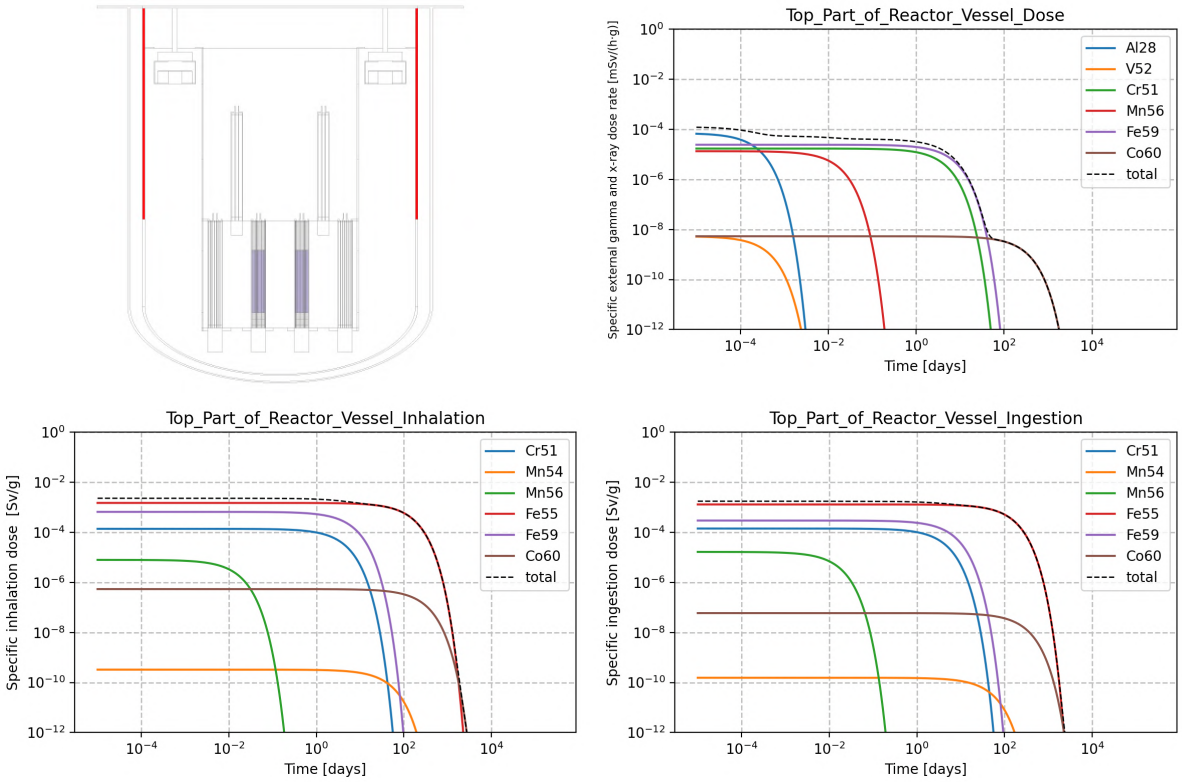


Figure 25: Results for the top part of the reactor vessel.

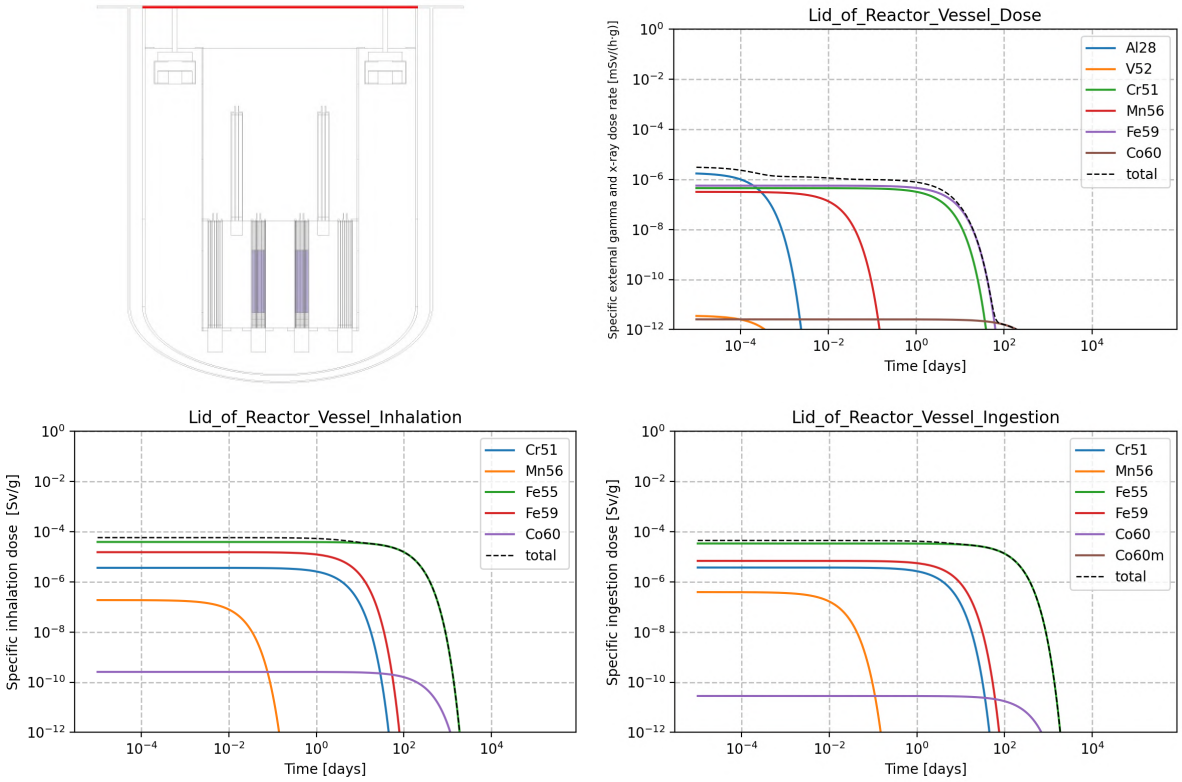


Figure 26: Results for the lid of the reactor vessel.

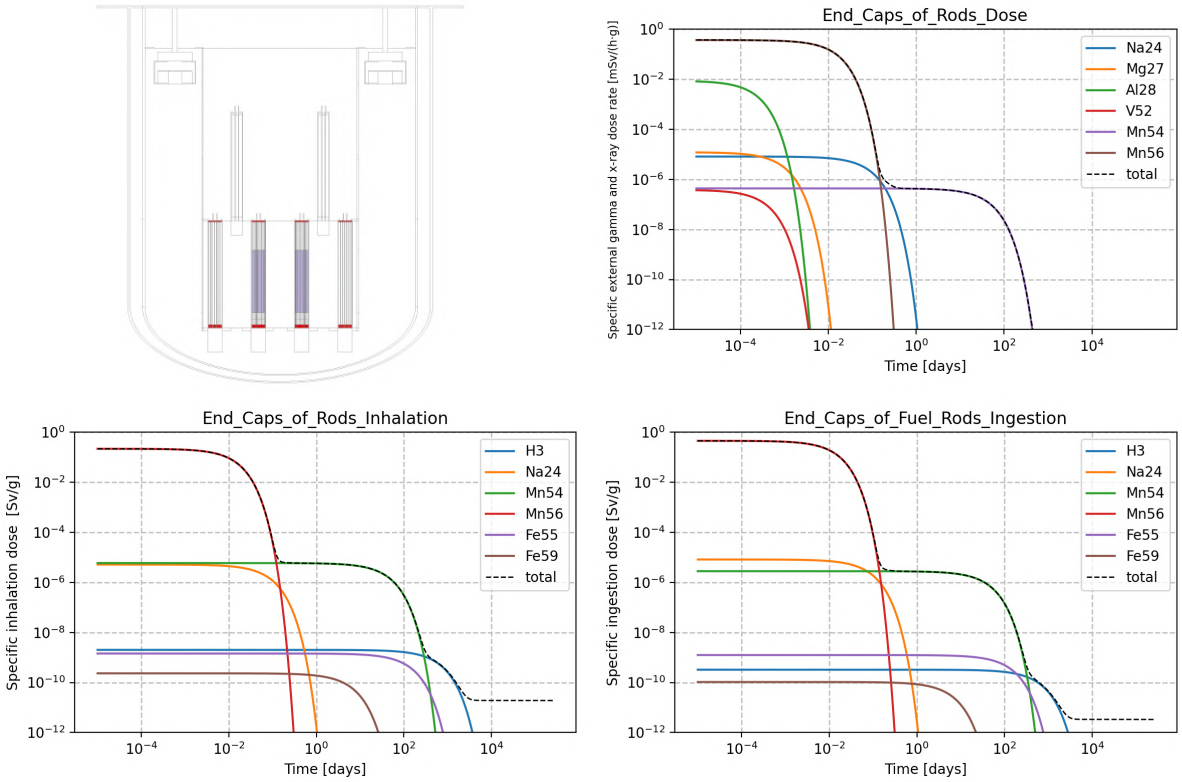


Figure 27: Results for the AFA in the end caps of the fuel and reflector rods.

The results in Figures 23, 24, 25, and 26 reveal a notable trend wherein predominant isotopes exhibit a decay time spanning approximately 3000 days. This observation implies that the cooling time for the reactor vessel is approximately eight to nine years. Regarding Figure 27, a distinct trend emerges, indicating a cooling duration of approximately 1000 days or equivalently three years for AFA. Consequently, the dominating isotopes for the cooling time of the reactor vessel come from the SS316L stainless steel and not from the AFA stainless steel.

### 4.2.2 Reactor Vessel - Clearance limit comparison

In this section, Figures 28 to 32 show those isotopes for the reactor vessel (and end caps) with specific activities exceeding the clearance limit threshold for the specific activity. In this case, the clearance limit pertains to iron-55 (Fe55) for Figures 23, 24, 25, 26 and, for the last figure (Figure 27) the safety limit refers to manganese-54 (Mn54).

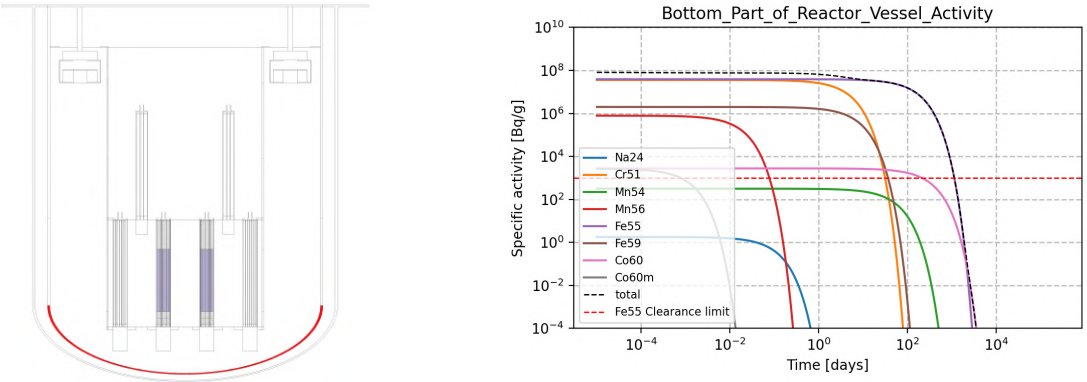


Figure 28: Results for the specific activity of the bottom of the reactor vessel.

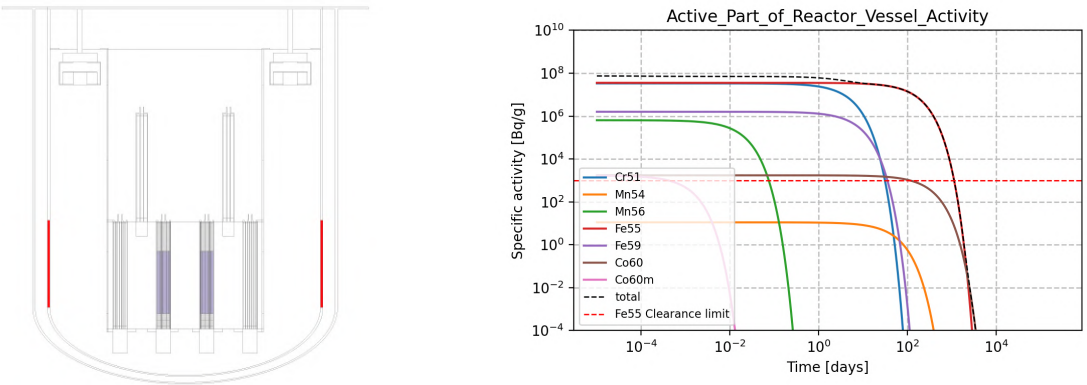


Figure 29: Results for the specific activity of the centre of the reactor vessel.

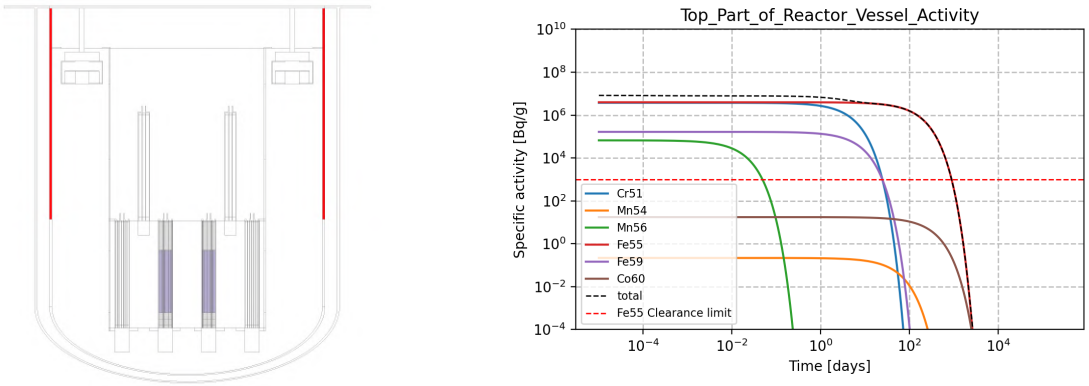


Figure 30: Results for the specific activity of the top part of the reactor vessel.

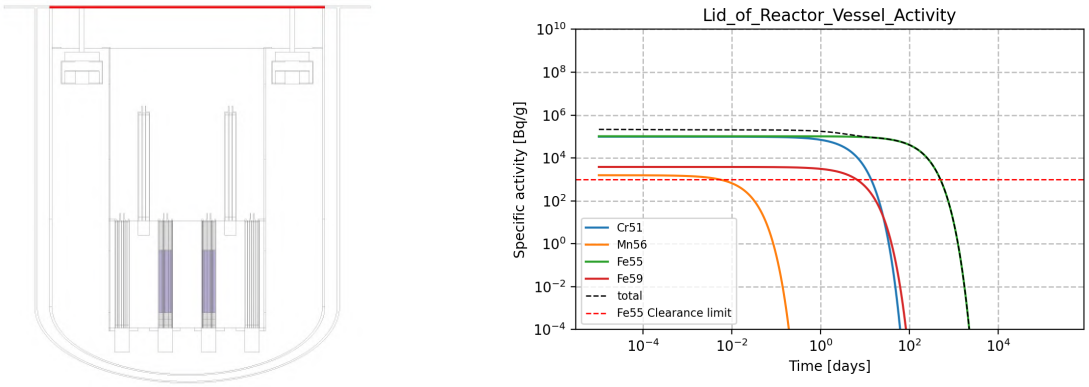


Figure 31: Results for the specific activity of the lid of the reactor vessel.

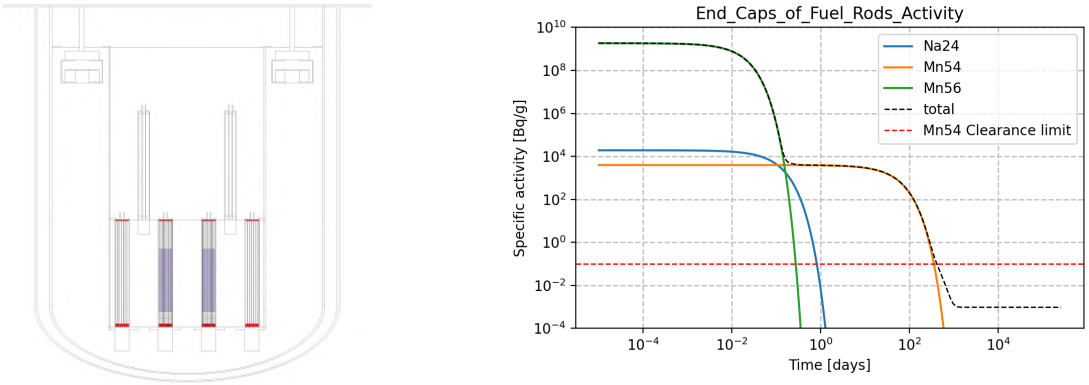


Figure 32: Results for the specific activity of the AFA in the end caps of the fuel and reflector rods.

On the one hand, we can see that the reactor vessel reaches a specific activity level below the safety limits within 3000 days. This outcome can be attributed to the presence of iron-55, a very active isotope that, despite its high activity, produces very little external dose. On the other hand, in the context of the end caps, it becomes

evident that safety levels are achieved within a comparatively shorter interval of 1000 days.

## 4.3 Steam Generator Unit

One important focus of this thesis is the examination of how the steam generators become activated. The first subsection will specifically focus on quantifying the external gamma and x-ray dose originating from a single unit. Subsequently, the second subsection will explore the radiotoxicity associated with the ingestion and inhalation of particles linked to the parts of the steam generator. It is possible that, in case of wanting to recycle the steam generators, personnel will have to dismantle the unit into smaller parts. This division aims to address the possibility of workers being exposed to dust ingestion or inhalation during the possible cutting procedure. In such an event, our objective is to evaluate the severity of the potential consequences. The unit has been partitioned into four distinct sections to facilitate the understanding of how each part gets activated.

### 4.3.1 Steam Generator Unit - External Gamma and X-ray Dose Rate

In Figure 33, we observe the rate at which external radiation is emitted by the entire steam generator unit. As anticipated, given that the steam generator primarily comprises FeCrAl, the introduction of niobium leads to the production of its long-lived radioactive isotope, niobium-94. Notably, the radiation dose stemming from this predominant isotope amounts to micro-Sieverts, a magnitude comparable to background radiation levels.

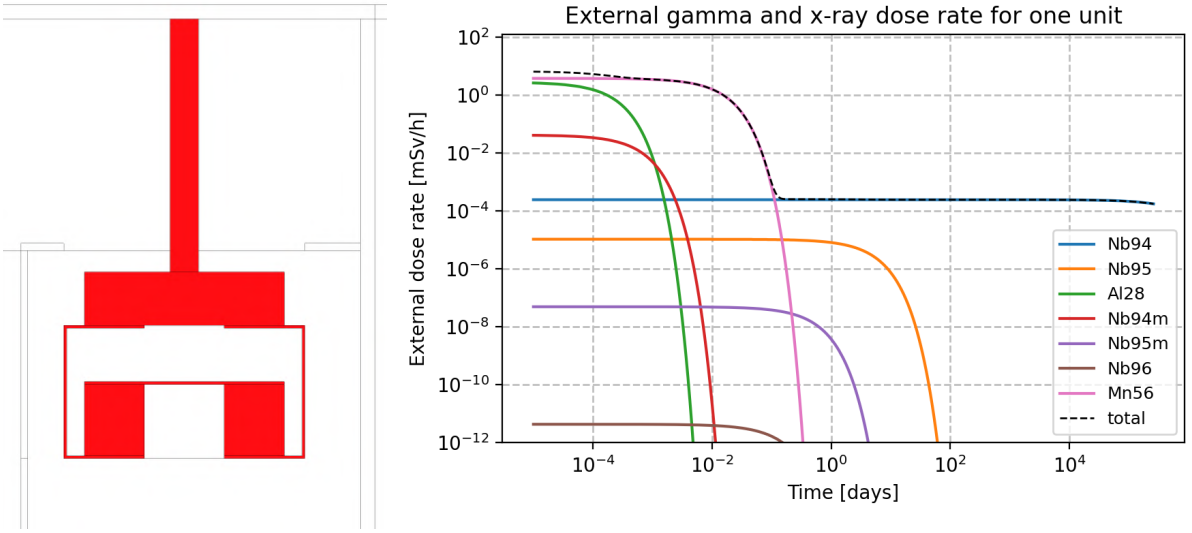


Figure 33: External dose in mSv/h for one steam generator.

### 4.3.2 Steam Generator Parts - Ingestion and Inhalation Radiotoxicity

This section presents the outcomes obtained for distinct segments of the steam generator. Figures 34 through 37 exclusively depict the doses for ingestion (left plot) and inhalation (right plot) associated with each individual component of the steam generator. In the event of segment dissection, prudent caution must be exercised to mitigate potential risks stemming from the ingestion or inhalation of particles released during the cutting process. In conclusion, as expected, the dominating dose comes from niobium-94. In this case, we exclusively present the doses related to ingestion and inhalation, as the total external dose rate is illustrated in Figure 33.

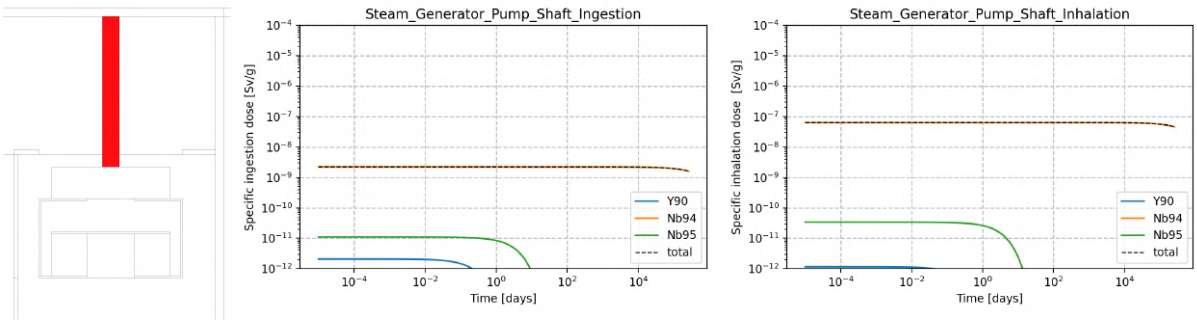


Figure 34: Results for ingestion and inhalation for the steam generator pump shaft.

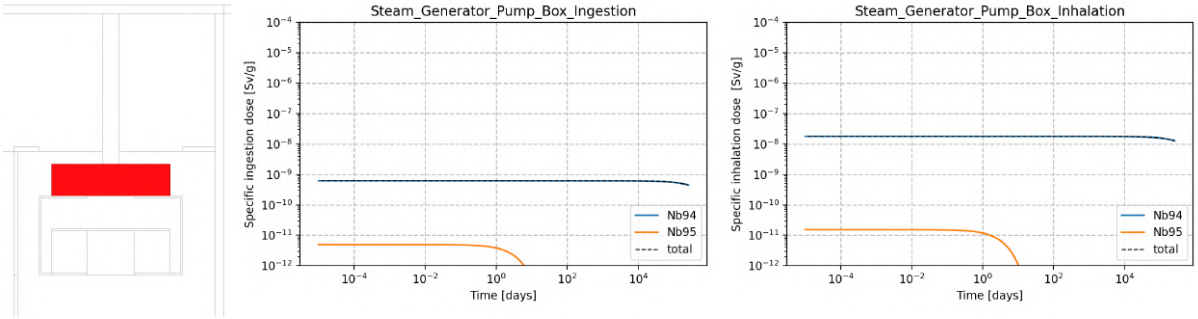


Figure 35: Results for ingestion and inhalation for the steam generator pump box.

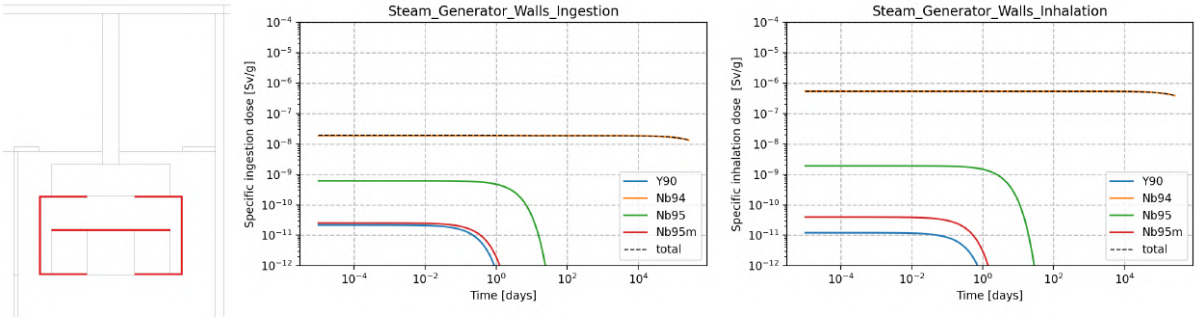


Figure 36: Results for ingestion and inhalation for the walls of the steam generator.

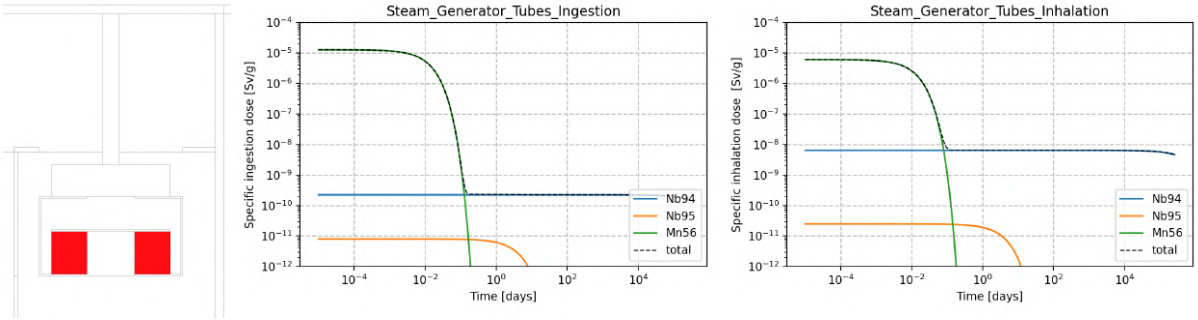


Figure 37: Results for ingestion and inhalation for the steam generator tubes.

## 4.4 Neutron and photon leakage

In this final section, we will examine the neutron and photon flux (expressed in units of particles $\cdot s^{-1} \cdot cm^{-2}$) that emanate from the nuclear reactor. These measurements have been obtained from detectors strategically positioned around the active region of the reactor core, specifically at a distance of half a meter away from the reactor vessel wall. Additionally, another detector has been situated on top of the reactor. This section will be divided into two distinct sections, one for the neutron flux and the other for the photon flux.

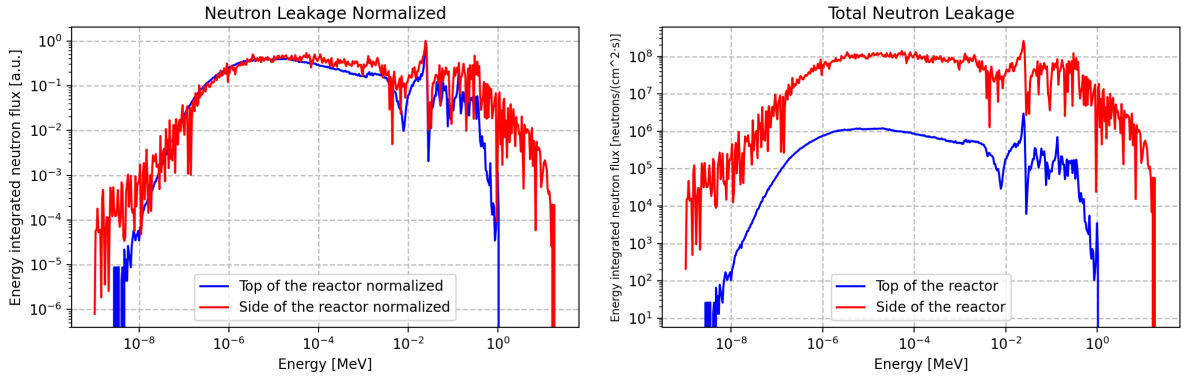


Figure 38: The plot on the left displays the energy-integrated neutron flux normalized to one for the detector on top of the reactor (blue) and the detector situated around the active core (red). On the right, the corresponding real values are depicted, representing the neutron flux in units of particles $\cdot$ $s^{-1}$ $\cdot$ $cm^{-2}$ for both cases as well. The x-axis represents the energy of the neutrons detected.

### 4.4.1 Neutron Leakage

In Figure 38, the energy-integrated neutron flux detected outside the reactor is depicted. The plot on the left displays the normalized energy-integrated neutron flux to one, whereas the plot on the right presents the actual counts registered by the detector. Within these plots, the red line represents neutron leakage from the reactor's lateral side, while the blue line corresponds to neutron leakage from the upper portion of the reactor. Meanwhile, in Figure 39, we can see the projected path of the neutrons on a 2D image of the reactor depicted as black lines. The image on the left shows a vertical cross-section of the reactor and the image on the right shows an horizontal cross-section. In other words, in the image on the left we are seeing the reactor from the side and, in the image on the right, we are seeing the reactor core from the top.

### 4.4.2 Photon Leakage

We detected a total of **zero** photos escaping the reactor core. Figure 40 shows the projected path of the photons generated inside the reactor core for the vertical (left) and horizontal (right) cross-sections.

Figure 39: The image on the left illustrates the vertical cross-section of the reactor, while the image on the right depicts the horizontal cross-section. The black lines in both images represent the projected paths of the simulated neutrons. While the majority of neutrons are confined within the core, a portion of them manages to escape the reactor.

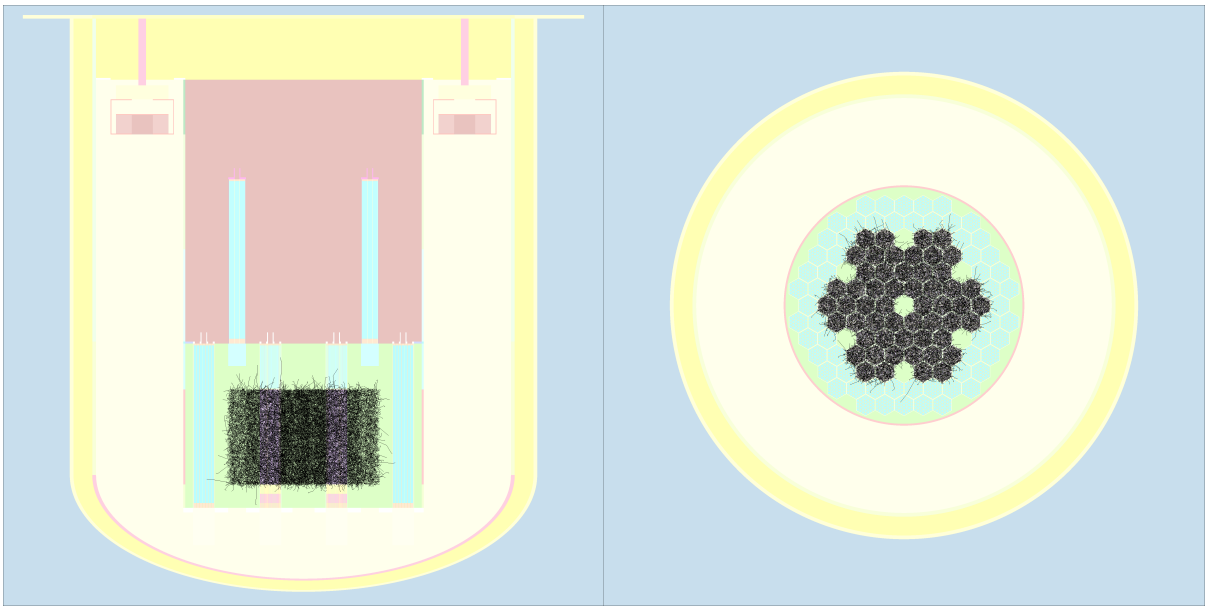

Figure 40: The image on the left illustrates the vertical cross-section of the reactor, while the image on the right depicts the horizontal cross-section. The black lines in both images represent the projected paths of the simulated photons. In comparison with Figure 39. all the photons are absorbed shortly after leaving the core.

# Chapter 5

# Discussions

The discussion section will adhere to the same section division as that of the results section. The initial segment will centre on the outcomes obtained for the activation of FeCrAl in the internal structures of the reactor, while the following part will concentrate on the activation of the AFA stainless steel and the cooling time for the reactor vessel. In the third section, we will examine the dose received from one steam generator unit after undergoing irradiation for one and a half years and its inhalation and ingestion radiotoxicity. Finally, the last section will discuss the disparity in the flux between the neutrons and gamma photons leaking from the reactor core.

## 5.1 Internal Structures of the Reactor - FeCrAl

From Figure 14 to Figure 22, it is evident that for all the investigated components, the specific activity of niobium-94 (Nb94) surpasses the limit prescribed in [3]. The extended half-life of niobium-94, which stands as the longest among all the activated isotopes studied in this thesis, measures $2.03 \cdot 10^4$ years [26]. Due to its long half-life and its specific activity exceeding the safety threshold, the recycling of components containing niobium-94 becomes impractical, necessitating its disposal as radioactive waste. Nevertheless, when analyzing the graphs situated in the upper right-hand corner for Figure 5 to Figure 13, detailing the specific external gamma and x-ray dose rates in $\mathrm{mSv} \cdot \mathrm{h}^{-1} \cdot \mathrm{g}^{-1}$, we observe that even for the most severe scenario, represented by the active portion of the core barrel in Figure 7, the value for niobium-94 is in the order of $10^{-4}$ $\mathrm{mSv} \cdot \mathrm{h}^{-1} \cdot \mathrm{g}^{-1}$. As per data from [29], the average background radiation stands at $2.4$ $\mathrm{mSv} \cdot \mathrm{y}^{-1}$, approximately equivalent to $2.7 \times 10^{-4}$ $\mathrm{mSv} \cdot \mathrm{h}^{-1}$. Despite this,

with appropriate treatment, structures positioned further away from the core, such as those given by Figures 11, 12, and 13, exhibit a significant reduction in specific external gamma and x-ray dose rates, potentially leading to a higher probability of recycling. Conversely, other isotopes showing higher external doses than niobium-94 undergo rapid decay. Notably, niobium-95 (Nb95) represents the second-longest half-life ($34.99$ days [26]) isotope and exhibits increased external doses in structures closer to the core (from Figure 5 to Figure 11). Nevertheless, niobium-95 experiences rapid decay, reaching negligible levels within approximately 100 days. The decline in niobium-95 concentration as one moves away from the core arises from a reduction of neutron flux, resulting in reduced neutron absorption.

## 5.2 Reactor Vessel - AFA

AFA stainless steel serves as a corrosion-resistant coating in the primary reactor vessel, which itself is constructed from SS316L stainless steel. The AFA coating is 200 microns thick, whereas SS316L has a thickness of 40 mm. This difference in thickness makes the quantity of AFA significantly smaller than SS316L. Due to its limited presence, we also examined the activation of AFA in the end caps of the fuel and reflector rods. In this specific case, the end caps, located at the top and bottom of the rods, consist entirely of pure AFA material. Notably, these end caps do not form part of any structural component or the reactor vessel. Nonetheless, exploring the activation of AFA in the end caps proves intriguing and useful information.

In Section 4.2.2, the red dashed line in Figures 28, 29, 30, and 31 corresponds to the threshold safety limit for the specific activity of iron-55 (Fe55), which is $1000$ Bq/g. Meanwhile, for Figure 32, the limit is manganese-54 (Mn54), which is $0.1$ Bq/g and has a half-life of $312.20$ days. Figures 28, 29, 30, and 31 show the dominance of iron-55 and chromium-51 (Cr51). It is noteworthy that chromium-51 (with a half-life of $27.70$ days [26]) exhibits rapid decay within 100 days, while iron-55 possesses a half-life of $2.774$ years [26]. Intriguingly, despite iron-55 dominating the specific activity, it does not manifest in the specific external gamma and x-ray dose rates in Figures 23, 24, 25, and 26. This observation indicates that although iron-55 exceeds the safety limit, its impact on the external dose remains insignificant. Conversely, iron-55 poses a highly perilous risk in cases of ingestion or inhalation. For the most severe scenarios, as depicted in Figures 23 and 24, the ingestion and inhalation dose for iron-55 is in the order of $10^{-2}$

Sv/g. Consequently, if the vessel is cut during decommissioning or recycling and dust particles containing this isotope are ingested or inhaled by personnel, severe damage can happen. Fortunately, within approximately 3000 days or eight to nine years, the isotope undergoes sufficient decay to reach safer levels, thereby mitigating the risk associated with its presence.

From all the aforementioned Figures, it is evident that SS316L stainless steel emerges as the dominant material. Consequently, the role of AFA remains relatively minor, given its minimal quantity. Despite this, Figures 27 and 32 portray the activation of pure AFA, despite it not being part of the reactor vessel. In Figure 32, manganese-56 (Mn56), with a half-life of $2.57$ h, prevails in terms of specific activity but rapidly decays within a day. Subsequently, manganese-54 dominates the specific activity for longer, yet it decays to safety limits before reaching 1000 days. A similar trend is observed in the plots of Figure 27, where manganese-56 dominates initially, followed by manganese-54 which prevails for roughly 1000 days. It is important to mention that Figures 27 and 32 represent part of the fuel and reflector assemblies, not the reactor vessel. After approximately three years, the dose emanating from AFA diminishes sufficiently to enable recycling. However, it is essential to reiterate that this AFA constitutes part of the fuel and reflector assembly, which will not be recycled due to the high dose emanating from the entire assembly.

## 5.3 Steam Generator Unit

The steam generators are treated as units, intended to be replaced annually. Consequently, understanding the dose emanating from the entire structure holds a significant interest. In Figure 33, the total external gamma and x-ray dose rate is presented. On the first day, manganese-56 emerges as the dominant isotope, contributing to an approximate dose of $10$ mSv/h. Subsequently, niobium-94 assumes dominance in the dose profile for the steam generator unit's entire lifespan. The external dose rate attributed to niobium-94 is on the order of $10^{-4}$ mSv/h, slightly surpassing background radiation levels. It is important to note that the present analysis does not account for self-shielding, implying that the real value of the external gamma and x-ray dose rate will be lower than the obtained result. As a consequence, handling the steam generator unit proves to be a highly viable option.

In section 4.3.2, Figures 34, 35, 36, and 37 illustrate that the predominant long-lived isotope is niobium-94. Consequently, if any of these parts are cut for recycling, particular attention to inhalation hazards becomes imperative. Nevertheless, it is essential to highlight that even though the highest inhalation dose is observed in the right plot of Figure 36, it amounts to approximately $10^{-6}$ Sv/g. This indicates that with meticulous care during the recycling process, the risk of severe damage can be effectively mitigated.

## 5.4 Neutron and photon leakage flux

This last section focuses on the neutron and photon flux leaving the reactor. In Figure 38 we can see the energy-integrated neutron flux. In the left plot, the lateral neutron flux (red) and the top neutron flux (blue) escaping the reactor are normalized to one. In the plot on the right, we see the real value of the flux (in neutons $\cdot$ cm$^{-2}$ $\cdot$ s$^{-1}$). We can see that the lateral neutron flux is higher than the top neutron flux. This makes sense since the top of the reactor is further away from the core than the lateral part of the reactor.

A slight thermalization of the neutrons is apparent in Figure 38, indicating the reduction of neutron energy due to interactions with the coolant. Due to the high mass of the lead atoms, elastic scattering interactions between neutrons and lead atoms result in negligible energy loss for the neutrons. Consequently, the thermalization of neutrons is not particularly prominent in the SUNRISE-LFR[1].

In Figure 39, the distinct trajectories of neutrons leaving the core are depicted as black lines. As anticipated, the densest neutron flux is observed at the core's centre. In contrast, Figure 40 displays the paths of photons, clearly illustrating their difference from the neutron behaviour. While neutrons can escape the reactor, high-energy photons exhibit limited range, ceasing propagation shortly after their release. It is pertinent to note that despite extensive simulation efforts, no photons were detected, reinforcing the notion that their presence is significantly constrained compared to neutrons in this particular reactor configuration.

[1]It is worth noting that greater thermalization would be anticipated in a light water reactor, as water serves as a more effective moderator compared to lead.

# Chapter 6

# Conclusions and Future Work

## 6.1 Conclusions

We can extract several conclusions from the results obtained in this thesis. Firstly, it is evident that all internal structures composed of FeCrAl as the bulk material exhibit a total specific activity surpassing the clearance limit [3]. The isotope primarily responsible for this excess is niobium-94, exhibiting a lengthy half-life of $2.03 \cdot 10^4$ years [26]. Thanks to its long half-life, the specific external gamma and x-ray dose rate originating from this particular isotope, even in the worst-case scenario (Figure 7, corresponding to the core barrel section next to the active core), amounts to $0.1$ $\mu$Sv, equivalent to background radiation levels, which is approximately $2.7 \cdot 10^{-4}$ mSv $\cdot$ $h^{-1}$ [29]. This observation indicates that with an appropriate recycling process, the internal structures can be efficiently and safely reused within the nuclear sector but since the limit surpasses the clearance limit it can not be reused for other non-nuclear applications.

Regarding the reactor vessel, its cooling time is primarily influenced by cobalt-60 and iron-55, both of which decay to negligible levels within approximately 3000 days (or eight to nine years). This cooling duration of nine years is manageable and presents no significant challenges. The main concern lies in the potential inhalation and ingestion of iron-55. As for AFA, the limited abundance in the main reactor vessel results in a minimal impact on the vessel's activation. Consequently, attention was directed to the end caps of the fuel and reflector rods. There, manganese-54 dominates the external specific dose rate but decays to negligible levels before reaching 1000

days.

In conclusion, both the reactor vessel and the internal structures can be readily treated and managed after a cooling period of nine years. The decay of relevant isotopes to safe levels within this timeframe ensures a secure handling process. For example, the reactor vessel can be stored in a warehouse for nine years, after this period, the reactor vessel can be recycled and released from radiological control.

In the case of the steam generator units, analysis reveals that the external dose rate emanating from a single unit after 1.5 years of exposure is predominantly influenced by niobium-94. However, the dose observed amounts to approximately $0.1$ $\mu$Sv/h, which aligns with the background radiation levels (approximately $0.27$ $\mu$Sv [29]). This observation indicates that the steam generator unit is safe to handle by personnel without significant concern.

In the event of considering cutting the steam generator, special protection against the ingestion or inhalation of particles is crucial, as niobium-94 predominantly dominates. Despite this, even in the worst-case scenario, which involves the inhalation of one gram of material in the form of particles originating from the steam generator walls, the specific inhalation dose remains on the order of $\mu$Sv/h.

Finally, our investigation reveals that the neutron flux outside the radial part of the reactor reaches approximately $10^8$ neutrons $\cdot$ cm$^{-2} \cdot$ s$^{-1}$, while, for the flux on top of the reactor, is $10^6$ neutrons $\cdot$ cm$^{-2} \cdot$ s$^{-1}$. It is essential to emphasize that this configuration represents the worst-case scenario. However, safety measures can be implemented to significantly reduce the external neutron lateral flux.

Indeed, the use of lead as a coolant has demonstrated remarkable effectiveness in attenuating high-energy photons within the reactor. Lead serves as a potent shield, effectively containing the high-energy photons and preventing their dispersion outside the reactor boundaries.

In summary, adopting suitable shielding strategies and protective coatings can play a pivotal role in safeguarding reactor operations, mitigating radiation risks, and ensuring the safe and efficient functioning of the reactor system. Such efforts are crucial for advancing nuclear safety standards and ensuring the well-being of personnel and the environment in and around the reactor facility.

## 6.2 Future Work

This thesis paves the way for several promising research directions. Investigating new FeCrAl compositions to minimize niobium-94 impact, studying activation in additional structural components, and exploring strategies to reduce neutron flux outside the reactor for personnel safety are key areas of interest. Moreover, better studies on the dose received by personnel can be implemented since the results for the neutron leakage obtained in this thesis only show the flux. In addition, it would be intriguing to study the amount of nuclear waste produced per kW/h for the SUNRISE reactor.

# Bibliography


[1] Ejenstam, Jesper, Halvarsson, Mats, Weidow, Jonathan, Jönsson, Bo, and Szakalos, Peter. "Oxidation studies of Fe10CrAl–RE alloys exposed to Pb at 550°C for 10,000h". In: *Journal of Nuclear Materials* 443.1 (2013), pp. 161–170. ISSN: 0022-3115. DOI: https://doi.org/10.1016/j.jnucmat.2013.07.023. URL: https://www.sciencedirect.com/science/article/pii/S0022311513009112.

[2] Ejenstam, Jesper and Szakálos, Peter. "Long term corrosion resistance of alumina forming austenitic stainless steels in liquid lead". In: *Journal of Nuclear Materials* 461 (2015), pp. 164–170. ISSN: 0022-3115. DOI: https://doi.org/10.1016/j.jnucmat.2015.03.011. URL: https://www.sciencedirect.com/science/article/pii/S0022311515001555.

[3] Yngvesson, Ulf. "Strålsäkerhetsmyndighetens föreskrifter om undantag från strålskyddslagen och om fri- klassning av material, byggnadsstrukturer och områden". In: (May 2018). ISSN: 2000-0987. URL: https://www.stralsakerhetsmyndigheten.se/contentassets/fd378df462fa47a58935551d27bace50/ssmfs-20183-stralsakerhetsmyndighetens-foreskrifter-om-undantag-fran-stralskyddslagen-och-om-friklassning-av-material-byggnadsstrukturer-och-omraden.pdf.

[4] Cook, John. "Consensus on consensus: a synthesis of consensus estimates on human-caused global warming". In: *Environmental Research Letters* (2016). DOI: 10.1088/1748-9326/11/4/048002. URL: https://iopscience.iop.org/article/10.1088/1748-9326/11/4/048002/pdf.

[5] McGrath, Matt. “Climate change: Biggest global poll supports global emergency”. In: (2021). URL: https://www.bbc.com/news/science-environment-55802902.

[6] “Environmental Impacts of Hydroelectric Power”. In: *Union of Concerned Scientists* (March 5, 2013). URL: https://www.ucsusa.org/resources/environmental-impacts-hydroelectric-power.

[7] Breyer, Christian, Khalili, Siavash, Bogdanov, Dmitrii, Ram, Manish, Oyewo, Ayobami Solomon, Aghahosseini, Arman, Gulagi, Ashish, Solomon, A. A., Keiner, Dominik, Lopez, Gabriel, Østergaard, Poul Alberg, Lund, Henrik, Mathiesen, Brian V., Jacobson, Mark Z., Victoria, Marta, Teske, Sven, Pregger, Thomas, Fthenakis, Vasilis, Raugei, Marco, Holttinen, Hannele, Bardi, Ugo, Hoekstra, Auke, and Sovacool, Benjamin K. “On the History and Future of 100% Renewable Energy Systems Research”. In: *IEEE Access* 10 (2022), pp. 78176–78218. DOI: 10.1109/ACCESS.2022.3193402.

[8] IEA. “Nuclear Power in a Clean Energy System”. In: (2019). URL: https://www.iea.org/reports/nuclear-power-in-a-clean-energy-system.

[9] *The Hisotry of Nuclear Energy*. URL: https://www.energy.gov/sites/prod/files/The%20History%20of%20Nuclear%20Energy_0.pdf.

[10] Josephson, Paul R. *Red Atom: Russia’s Nuclear Power Program from Stalin to Today*. University of Pittsburgh, 2005.

[11] “Nuclear Power in the World Today”. In: (March 2023). URL: https://world-nuclear.org/information-library/current-and-future-generation/nuclear-power-in-the-world-today.aspx.

[12] “The Ultimate Fast Facts Guide to Nuclear Energy”. In: (2019). URL: https://www.osti.gov/biblio/1545613.

[13] “Majority in Japan backs nuclear power for first time since Fukushima”. In: (2022). URL: https://www.japantimes.co.jp/news/2022/03/28/national/nuke-power-poll/.

[14] Analysgruppen. “OPINION POLLS”. In: (2022). URL: https://www.analys.se/engelska/opinion-polls/.

[15] SAAD, LYDIA. “Americans Divided on Nuclear Energy”. In: (2022). URL: https://news.gallup.com/poll/392831/americans-divided-nuclear-energy.aspx.

[16] SSF. “Nuclear Power in a Clean Energy System”. In: (August 2019). URL: https://strategiska.se/app/uploads/arc19_en.pdf.

[17] “Transforming our world: the 2030 Agenda for Sustainable Development”. In: (2023). URL: https://sdgs.un.org/2030agenda.

[18] Dehlin, Fredrik, Wallenius, Janne, and Bortot, Sara. “An analytic approach to the design of passively safe lead-cooled reactors”. In: *Annals of Nuclear Energy* 169 (2022), p. 108971. ISSN: 0306-4549. DOI: https://doi.org/10.1016/j.anucene.2022.108971.

[19] Leppänen, Jaakko, Pusa, Maria, Viitanen, Tuomas, Valtavirta, Ville, and Kaltiaisenaho, Toni. “The Serpent Monte Carlo code: Status, development and applications in 2013”. In: *Annals of Nuclear Energy* 82 (2015), pp. 142–150. ISSN: 0306-4549. DOI: https://doi.org/10.1016/j.anucene.2014.08.024. URL: https://www.sciencedirect.com/science/article/pii/S0306454914004095.

[20] John R. Lamarsh, Anthony J. Baratta. *Introduction to Nuclear Engineering*. 3rd ed. Upper Saddle River, New Jersey 07458: Prentice Hall, 2001.

[21] “Physics of Uranium and Nuclear Energy”. In: (February 2022). URL: https://world-nuclear.org/information-library/nuclear-fuel-cycle/introduction/physics-of-nuclear-energy.aspx.

[22] Sublet, Jean-Christophe, Fleming, Michael, and Gilbert, Mark. “From cutting-edge pointwise cross-section to groupwise reaction rate: A primer”. In: *EPJ Web of Conferences* 146 (Jan. 2017), p. 02003. DOI: 10.1051/epjconf/201714602003.

[23] (GIF), Generation IV International Forum. “GIF 2021 Annual Report”. In: (2021). URL: https://www.gen-4.org/gif/jcms/c_203335/gif-2021-ar.

[24] IAEA. *Advanced Reactors Information System(ARIS)*. URL: https://aris.iaea.org/sites/RPV.html.

[25] IAEA. *Small modular reactors: flexible and affordable power generation*. URL: https://www.iaea.org/topics/small-modular-reactors.

[26] IAEA. *Live Chart of Nuclides*. URL: https://www-nds.iaea.org/relnsd/vcharthtml/VChartHTML.html.

[27] Peplow, Douglas E. "Specific Gamma-Ray Dose Constants with Current Emission Data". In: *Health Physics* 118.4 (Apr. 2020). DOI: 10.1097/HP.0000000000001136.

[28] Greenwood, L R. "Neutron interactions and atomic recoil spectra". In: (Aug. 1993). URL: https://www.osti.gov/biblio/10111988.

[29] nuclear, world. *Some comparative whole-body radiation doses and their effects*. URL: https://www.world-nuclear.org/uploadedfiles/org/wna/publications/nuclear_information/pocket_guide_radiation.pdf.


Grenoble INP
phelma


KTH
VETENSKAP
OCH KONST


SUNRISE
Sustainable Nuclear Energy
Research in Sweden